Modeling, Analysis and Control of Ethylene Glycol Reactive Distillation Column

Aditya Kumar and Prodromos Daoutidis
Dept. of Chemical Engineering and Materials Science, University of Minnesota, Minneapolis, MN 55455

The dynamic behavior and control of an ethylene glycol reactive distillation column were studied. A detailed tray-by-tray model that explicitly includes the vapor-phase balances is derived and compared with a conventional model that ignores the vapor holdup. The steady-state variation of the product purity (the key output to be controlled) with respect to reboiler heat duty was studied, identifying a region of output multiplicity with three branches corresponding to different conversion and product selectivity. Further analysis of the process on the steady-state branch with high conversion and selectivity reveals a transition from minimum phase behavior at moderate purity to nonminimum phase behavior at high purity. The nonminimum phase behavior was analyzed and addressed in the design of a nonlinear inversion-based controller that performs well with stability in the high purity region.

Introduction

Reactive distillation, the process of simultaneous reaction and distillation in a single unit, offers numerous advantages over conventional configurations of reactors followed by separators. Unlike conventional reactor-separator configurations, in reactive distillation the reactants/products are continuously separated from the liquid reaction phase into the nonreactive vapor phase. This key feature allows an enhanced conversion in equilibrium limited reversible reactions (such as production of methyl/ethyl acetate), a higher product selectivity in the case of multiple competing reactions (such as production of ethylene glycol), and provides an efficient means of heat removal from (or heat addition to) the liquid phase for reactions with high heat of reaction. These advantages have motivated a renewed interest in the use of reactive distillation technology for the production of important chemicals (Agreda et al., 1990; DeGarmo et al., 1992). However, the interaction between the simultaneous reaction and distillation introduces a much more complex behavior compared to conventional reactors and ordinary distillation columns, and leads to challenging problems in design, operation, and control.

Initial research on reactive distillation focused mainly on the numerical simulation of steady-state profiles (Chang and Seader, 1988; Jelínek and Hlavàček, 1976). More recent research focused on analyzing the phase diagrams and studying the existence of azeotropes in multicomponent mixtures in the presence of reversible reactions at equilibrium (Barbosa and Doherty, 1988c; Ung and Doherty, 1995b) or with finite kinetics (Rév, 1994), using transformed coordinates that denote ''reaction-invariant'' composition variables. The design of reactive distillation columns with thermally neutral reversible reactions at equilibrium has been addressed using these reaction-invariant coordinates and residue curve maps (for a general survey, see Barbosa and Doherty, 1998a,b; Espinosa et al., 1995; Ung and Doherty, 1995a; Doherty and Buzad, 1992), while an approach for the design of columns with a kinetically limited reversible reaction was proposed in Buzad and Doherty (1994) using fixed-point methods. On the other hand, the design of columns with kinetically limited multiple reactions and significant heat effects has been addressed through nonlinear optimization on the basis of detailed steady-state models (Ciric and Gu, 1994; Pekkanen, 1995). In a different vein, research has also focused on the steady-state analysis of reactive distillation columns, establishing the existence of multiple steady states in columns with a single product stream (Pisarenko et al., 1988), MTBE column (Güttinger and Morari, 1997; Hauan et al., 1995; Jacobs and Krishna, 1993; Nijhuis et al., 1993), and ethylene glycol column (Ciric and Miao, 1994; Gehrke and Marquardt, 1997; Kumar and Daoutidis, 1995b). These results are indicative of the strong nonlinearities arising from the coupled reaction and distillation.

Correspondence concerning this article should be addressed to P. Daoutidis.

In contrast with steady-state simulation and design, dynamic modeling and simulation of reactive distillation columns received attention only recently where initial studies were based on simplified models consisting of only the material balance equations for columns with simultaneous phase and reaction equilibrium (Espinosa et al., 1994; Grosser et al., 1987; Moe et al., 1995). More recent work addressed the simulation of columns with kinetically limited reactions on the basis of more detailed models with material and energy balances (Alejski and Duprat, 1996; Ruiz et al., 1995). Despite increasing attention to dynamic modeling and simulation, available literature on control of reactive distillation columns is very limited. The early work of Roat et al. (1986) demonstrated the inadequacies of conventional linear multiloop controllers with input-output pairings based on steady-state interaction measures, and highlighted the need for more advanced controllers designed on the basis of rigorous dynamic models. In our previous work (Kumar and Daoutidis, 1995a), a detailed dynamic model was derived and used for the design of a nonlinear controller for a column with a kinetically limited reversible reaction. The control of batch reactive distillation columns has also been studied in the framework of optimal control (Sørensen et al., 1996) and nonlinear model predictive control using reduced-order models (Balasubramhanya and Doyle III, 1998). Recently, a strategy for the startup and continuous operation of an ethyl acetate column using a linear dynamic matrix control method was proposed in Baldon et al. (1997).

In this article, we address the dynamic modeling and nonlinear control of an ethylene glycol reactive distillation column. Initially, motivated by the consideration that the vapor holdup in a reactive distillation column may have a significant role in the coupled reaction-distillation dynamics (Kumar and Daoutidis, 1995a,b), we derive a detailed dynamic model which explicitly includes the vapor-phase dynamic balances and compare the dynamic behavior predicted by this model with that of a conventional model obtained under the assumption of negligible vapor holdup. We also perform a bifurcation analysis to investigate the existence of multiple steady states, focusing in particular on control-relevant input and output multiplicities, where the bottom product purity is the key output to be controlled. The study reveals a general three-branch output multiplicity and the existence of up to five steady states, indicating a complex nonlinear behavior. Furthermore, on the steady-state branch where it is desired to operate the column owing to the high conversion and selectivity, the column exhibits a transition from a minimum phase behavior at moderate purity to a nonminimum phase behavior at high purity. This nonminimum phase behavior imposes severe restrictions on the stability and performance characteristics of standard linear and nonlinear controllers. More specifically, we illustrate through simulations that the performance of conventional linear PI controllers leaves significant scope for improvement. On the other hand, standard inversion-based nonlinear controllers lead to closed-loop instability. Motivated by this, we address the design of a nonlinear controller that yields good performance at high purity with closed-loop stability. The controller design is pursued with the aid of a physical insight into the nonminimum phase behavior, and the performance of the controller is studied through simulations.

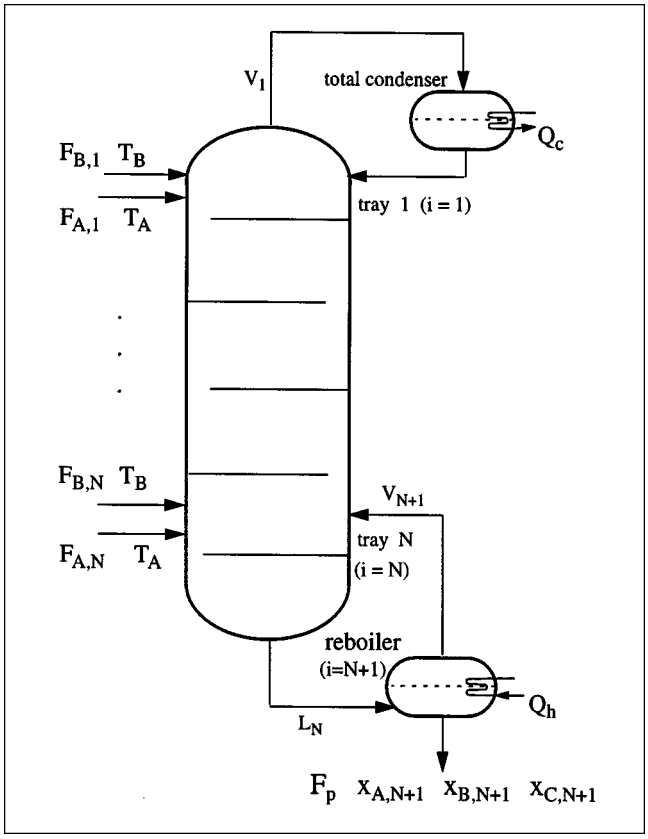

Figure 1. Ethylene glycol reactive distillation column.

Process Description and Modeling

We consider a general column with N trays (see Figure 1), where ethylene oxide (A) and water (B) are fed to stage i at molar flow rates $F_{A,i}$ and $F_{B,i}$, respectively, and the following liquid-phase reaction

$$C_2H_4O + H_2O \rightarrow C_2H_6O_2 \tag{1}$$

yields the main product, ethylene glycol (C). Ethylene glycol further reacts with unreacted ethylene oxide to produce diethylene glycol (D), a waste byproduct

$$C_2H_6O_2 + C_2H_4O \rightarrow C_4H_{10}O_3 \tag{2}$$

The kinetic data for the uncatalyzed reactions are obtained from Corrigan and Miller (1968) and Lichtenstein and Twigg (1948). Both reactions are quite slow at room temperature and their rates vary significantly with temperature. The rates of production of ethylene glycol in the main reaction (Eq. 1), $r_{1,i}$, and diethylene glycol in the secondary reaction (Eq. 2), $r_{2,i}$ on stage i are given by the following Arrhenius relations

$$r_{1,i} = 3.255 \times 10^{12} \exp\left(\frac{-9547.7}{T_i}\right) x_{A,i} x_{B,i} V_i \quad \text{(mol/s)}$$

$$r_{2,i} = 5.93 \times 10^{12} \exp\left(\frac{-9547.7}{T_i}\right) x_{A,i} x_{C,i} V_i \quad \text{(mol/s)} \tag{3}$$

where $x_{A,i}$, $x_{B,i}$ and $x_{C,i}$ are the mole fractions of ethylene

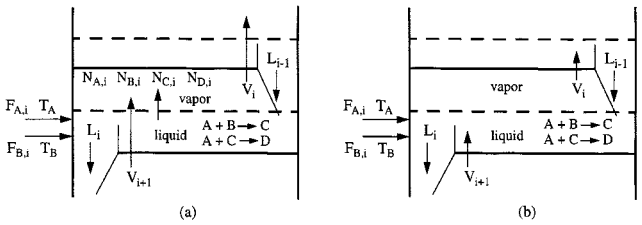

Figure 2. Vapor and liquid flow in a stage *i* (a) with vapor holdup, and (b) without vapor holdup.

oxide, water and ethylene glycol in the liquid phase, respectively, V_i (m^3) is the volume of the liquid holdup given by M_i^l/ρ_i^l, M_i^l is the molar liquid holdup, ρ_i^l is the average liquid molar density, and T_i is the temperature. Both reactants, ethylene oxide and water, are lighter than the products. Thus, unreacted ethylene oxide and water move up the column as more products are formed, and are completely recycled through a total condenser. The heavy products, ethylene glycol and diethylene glycol, are withdrawn at the bottom from the partial reboiler at a molar flow rate F_p.

For ordinary (nonreactive) distillation columns, dynamic models are derived under the standard assumptions of well-mixed liquid and vapor phases in thermodynamic equilibrium, and a negligible vapor holdup. The assumption of negligible vapor holdup is reasonably valid at low column pressures. However, in reactive distillation columns with exothermic reactions, the temperature and, hence, the pressure in the individual stages may be significantly high. Furthermore, even at low column pressures, the vapor holdup in the individual stages of a reactive distillation column may have an important role in the coupled reaction-separation dynamics. More specifically, a key feature of reactive distillation is the continuous separation of specific reactants/products from the liquid reaction phase into the nonreactive vapor phase on each stage i to promote high reactant conversion, product selectivity, and so on. The assumption of negligible vapor holdup is clearly contrary to this, since it implies that the vapor stream from a stage i directly enters the liquid phase, that is, the reaction phase, on stage $i-1$ (see Figure 2 for an illustration), defeating the separation of the reactants/products on stage i.

Motivated by the above observations, a detailed dynamic model of the ethylene glycol column is derived under the assumption of well-mixed ideal liquid and vapor phases at equilibrium. The model consists of a set of coupled differential and algebraic equations (DAEs) for each stage i, where the differential equations include the total and component mole balances in the liquid *and* vapor phases and the overall enthalpy balance, while the algebraic equations include the phase equilibrium relations, the ideal gas equation, the pressure drop correlation (Eckert and Kubíček, 1994), and the Francis weir formula. The resulting DAE model for stage i is given by

$$\dot{M}_i^v = V_{i+1} - V_i + N_{A,i} + N_{B,i} + N_{C,i} + N_{D,i} \tag{4}$$

$$\dot{y}_{A,i} = \frac{1}{M_i^v}\left[V_{i+1}(y_{A,i+1} - y_{A,i}) + N_{A,i}(1 - y_{A,i}) - (N_{B,i} + N_{C,i} + N_{D,i})y_{A,i}\right] \tag{5}$$

$$\dot{y}_{B,i} = \frac{1}{M_i^v}\left[V_{i+1}(y_{B,i+1} - y_{B,i}) + N_{B,i}(1 - y_{B,i}) - (N_{A,i} + N_{C,i} + N_{D,i})y_{B,i}\right] \tag{6}$$

$$\dot{y}_{C,i} = \frac{1}{M_i^v}\left[V_{i+1}(y_{C,i+1} - y_{C,i}) + N_{C,i}(1 - y_{C,i}) - (N_{A,i} + N_{B,i} + N_{D,i})y_{C,i}\right] \tag{7}$$

$$\dot{M}_i^l = F_{A,i} + F_{B,i} + L_{i-1} - L_i - r_{1,i} - r_{2,i} - N_{A,i} - N_{B,i} - N_{C,i} - N_{D,i} \tag{8}$$

$$\dot{x}_{A,i} = \frac{1}{M_i^l}\left[F_{A,i}(1 - x_{A,i}) - F_{B,i}x_{A,i} + L_{i-1}(x_{A,i-1} - x_{A,i}) - (r_{1,i} + r_{2,i})(1 - x_{A,i}) - N_{A,i}(1 - x_{A,i}) + (N_{B,i} + N_{C,i} + N_{D,i})x_{A,i}\right] \tag{9}$$

$$\dot{x}_{B,i} = \frac{1}{M_i^l}\left[-F_{A,i}x_{B,i} + F_{B,i}(1 - x_{B,i}) + L_{i-1}(x_{B,i-1} - x_{B,i}) - r_{1,i}(1 - x_{B,i}) + r_{2,i}x_{B,i} - N_{B,i}(1 - x_{B,i}) + (N_{A,i} + N_{C,i} + N_{D,i})x_{B,i}\right] \tag{10}$$

$$\dot{x}_{C,i} = \frac{1}{M_i^l}\left[-(F_{A,i} + F_{B,i})x_{C,i} + L_{i-1}(x_{C,i-1} - x_{C,i}) + r_{1,i}(1 + x_{C,i}) - r_{2,i}(1 - x_{C,i}) - N_{C,i}(1 - x_{C,i}) + (N_{A,i} + N_{B,i} + N_{D,i})x_{C,i}\right] \tag{11}$$

$$\dot{T}_i = \frac{1}{M_i^l cp_i^l + M_i^v cp_i^v}\left[F_{A,i}cp_A(T_A - T_i) + F_{B,i}cp_B(T_B - T_i) + V_{i+1}cp_{i+1}^v(T_{i+1} - T_i) + L_{i-1}cp_{i-1}^l(T_{i-1} - T_i) - (N_{A,i}\Delta H_A^v + N_{B,i}\Delta H_B^v + N_{C,i}\Delta H_C^v + N_{D,i}\Delta H_D^v) - r_{1,i}(\Delta H_{r1}^o + \Delta cp_1(T_i - T_o)) - r_{2,i}(\Delta H_{r2}^o + \Delta cp_2(T_i - T_o))\right] \tag{12}$$

$$0 = P_i y_{A,i} - P_{A,i}^s x_{A,i} \tag{13}$$

$$0 = P_i y_{B,i} - P_{B,i}^s x_{B,i} \tag{14}$$

$$0 = P_i y_{C,i} - P_{C,i}^s x_{C,i} \tag{15}$$

$$0 = P_i y_{D,i} - P_{D,i}^s x_{D,i} \tag{16}$$

$$0 = P_i\left(V_t - \frac{M_i^l}{\rho_i^l}\right) - M_i^v RT_i \tag{17}$$

$$0 = P_i - P_{i-1} - \sigma_1\left(\frac{V_i RT_i}{P_i}\right)^2 - \sigma_2\left(\frac{M_{i-1}^l}{\rho_{i-1}^l}\right) \tag{18}$$

$$0 = L_i - 1.839W\rho_i^l\left(\frac{M_i^l - \rho_i^l V_w}{\rho_i^l A}\right)^{1.5} \tag{19}$$

where M_i^v is the molar vapor holdup, and $y_{A,i}$, $y_{B,i}$, $y_{C,i}$ and $y_{D,i} = 1 - y_{A,i} - y_{B,i} - y_{C,i}$ are the mole fractions of the individual components in the vapor phase in equilibrium with the liquid phase at a temperature T_i and a pressure P_i. $N_{A,i}$, $N_{B,i}$,

$N_{C,i}$ and $N_{D,i}$ denote the molar rates of transfer of the respective components from the liquid to the vapor phase, while L_i and V_i are the molar flow rates of the liquid and vapor streams leaving the stage. In the ideal phase equilibrium relations (Raoult's law), the saturation vapor pressures of the components are evaluated by the standard Antoine relations

$$P^s_{A,i} = \exp\left(21.521 - \frac{2477.331}{T_i - 35.9}\right) \tag{20}$$

$$P^s_{B,i} = \exp\left(23.235 - \frac{3748.77}{T_i - 52.9}\right) \tag{21}$$

$$P^s_{C,i} = \exp\left(42.989 - \frac{34952.80}{T_i + 650.56}\right) \tag{22}$$

$$P^s_{D,i} = \exp\left(43.392 - \frac{35138.88}{T_i - 586.13}\right) \tag{23}$$

For the enthalpy balance, pure liquid component at a temperature of $T_o = 273$ K is used as the reference for evaluating the enthalpies of the ideal liquid and vapor mixtures. The heat of the reactions in Eq. 1 and Eq. 2 at the reference temperature T_o are $\Delta H^o_{r1} = -80$ kJ/mol and $\Delta H^o_{r2} = -13.1$ kJ/mol, while the molar heat capacity differences $\Delta cp_1 = cp_C - cp_A - cp_B$ and $\Delta cp_2 = cp_D - cp_A - cp_C$ describe the variation with temperature. Moreover, cp^l_i and cp^v_i are the average liquid- and vapor-phase molar heat capacities, ρ^l_i is the average liquid molar density, and ΔH^v_i denotes the average molar latent heat of vaporization.

In the modeling equations for the top tray (stage 1), there is no pressure drop correlation. Instead, for the case of total condenser with total recycle, the vapor flow rate V_1 is given by $V_1 = Q_c/\Delta H^v_1$, where Q_c is the heat duty in the condenser. Thus, the modeling equations for the top tray are obtained by setting $L_{i-1} = V_i$, $x_{A,i-1} = y_{A,i}$, $x_{B,i-1} = y_{B,i}$, $x_{C,i-1} = y_{C,i}$, and $T_{i-1} = T_i$. Similarly, the modeling equations for the partial reboiler (stage $N+1$) are obtained by setting $F_{A,i}$, $F_{B,i}$, $V_{i+1} = 0$ and $L_i = F_p$, including the heat input Q_h in the energy balance equation, and eliminating the Francis weir formula in Eq. 19.

These differential and algebraic equations (Eqs. 4 to 19) for each stage i together comprise the overall dynamic model for the column. It can be verified that this overall DAE model has an index two. Loosely speaking, the index of a DAE system is defined as the number of differentiations required to obtain a set of differential equations for all the variables in the system (for a more precise definition of index and a detailed discussion, see Brenan et al., 1996; Kumar and Daoutidis, 1995c). In the above model of the column, the interphase mole transfer rates are unknown (algebraic) variables that do not appear in any of the algebraic equations. Thus, the algebraic equations are singular in the sense that they cannot be solved directly for the interphase mole transfer rates, and have to be differentiated once to obtain a solution for these interphase mole transfer rates (see the controller design section).

Under the additional assumption of a negligible vapor holdup in each stage, the dynamic conservation equations for the vapor phase and, consequently, the interphase mole transfer rates are eliminated, to obtain the following DAE model for stage i

$$\dot{M}^l_i = F_{A,i} + F_{B,i} + L_{i-1} + V_{i+1} - L_i - V_i - r_{1,i} - r_{2,i} \tag{24}$$

$$\dot{x}_{A,i} = \frac{1}{M^l_i}\big[F_{A,i}(1 - x_{A,i}) - F_{B,i}x_{A,i} + L_{i-1}(x_{A,i-1} - x_{A,i}) + V_{i+1}(y_{A,i+1} - x_{A,i}) - V_i(y_{A,i} - x_{A,i}) - (r_{1,i} + r_{2,i})(1 - x_{A,i})\big] \tag{25}$$

$$\dot{x}_{B,i} = \frac{1}{M^l_i}\big[-F_{A,i}x_{B,i} + F_{B,i}(1 - x_{B,i}) + L_{i-1}(x_{B,i-1} - x_{B,i}) + V_{i+1}(y_{B,i+1} - x_{B,i}) - V_i(y_{B,i} - x_{B,i}) - r_{1,i}(1 - x_{B,i}) + r_{2,i}x_{B,i}\big] \tag{26}$$

$$\dot{x}_{C,i} = \frac{1}{M^l_i}\big[-(F_{A,i} + F_{B,i})x_{C,i} + L_{i-1}(x_{C,i-1} - x_{C,i}) + V_{i+1}(y_{C,i+1} - x_{C,i}) - V_i(y_{C,i} - x_{C,i}) + r_{1,i}(1 + x_{C,i}) - r_{2,i}(1 - x_{C,i})\big] \tag{27}$$

$$\dot{T}_i = \frac{1}{M^l_i cp^l_i}\big[F_{A,i}cp_A(T_A - T_i) + F_{B,i}cp_B(T_B - T_i) + L_{i-1}cp^l_{i-1}(T_{i-1} - T_i) + V_{i+1}cp^v_{i+1}(T_{i+1} - T_i) + V_{i+1}\Delta H^v_{i+1} - V_i\Delta H^v_i - r_{1,i}(\Delta H^o_{r1} + \Delta cp_1(T_i - T_0)) - r_{2,i}(\Delta H^o_{r2} + \Delta cp_2(T_i - T_0))\big] \tag{28}$$

$$0 = P_i y_{A,i} - P^s_{A,i}x_{A,i} \tag{29}$$

$$0 = P_i y_{B,i} - P^s_{B,i}x_{B,i} \tag{30}$$

$$0 = P_i y_{C,i} - P^s_{C,i}x_{C,i} \tag{31}$$

$$0 = P_i(1 - y_{A,i} - y_{B,i} - y_{C,i}) - P^s_{D,i}(1 - x_{A,i} - x_{B,i} - x_{C,i}) \tag{32}$$

$$0 = P_i - P_{i-1} - \sigma_1\left(\frac{V_i RT_i}{P_i}\right)^2 - \sigma_2\left(\frac{M^l_{i-1}}{\rho^l_{i-1}}\right) \tag{33}$$

$$0 = L_i - 1.839W\rho^l_i\left(\frac{M^l_i - \rho^l_i V_w}{\rho^l_i A}\right)^{1.5} \tag{34}$$

Note that in the above DAE model, the algebraic equations can be explicitly solved for the variables P_i, $y_{A,i}$, $y_{B,i}$, $y_{C,i}$, V_i and L_i. Thus, in this case, the overall DAE model for the column has an index one and can be directly reduced to an ODE model.

Steady-State Multiplicity and Dynamic Behavior

In the remainder of this article, we focus on a column with $N = 7$ trays, a single water feed $F_{B,1}$ to the top tray, and a single ethylene oxide feed $F_{A,4}$ to the fourth tray. For this column, we analyze the existence of multiple steady states and study the stability of the steady states on the basis of the linearized model. Note that at steady state, the index-two DAE model (Eqs. 4 to 19) reduces to the index-one model (Eqs. 24 to 34), that is, the two models have exactly the same

steady states; this can be verified by obtaining the relations for the interphase mole transfer rates $N_{A,i}, \ldots, N_{D,i}$ from the vapor-phase equations (Eqs. 4 to 7) at steady state. Thus, the simpler index-one DAE model can be used for steady-state analysis, simulation, and design purposes.

The steady-state overall material balance for the column yields the following for the total conversion of water (B)

$$F_{B,1} - F_p x_{B,N+1} = F_p(x_{C,N+1} + x_{D,N+1}) \qquad (35)$$

Thus, the product flow rate F_p is not an independent variable; it varies with the product composition according to the relation

$$F_p = \frac{F_{B,1}}{1 - x_{A,N+1}} \qquad (36)$$

This variation in F_p is incorporated in the analysis by controlling the liquid holdup M^l_{N+1} in the reboiler, using F_p as the manipulated input. Furthermore, the condenser heat duty Q_c is used to control the pressure in the top tray at one atmosphere. Under these specifications, there are altogether three degrees of freedom left in the column, the reactant feed flow rates $F_{B,1}$, $F_{A,4}$ and the reboiler heat duty Q_h, which will be varied to investigate the existence of multiple steady states in the column.

Initially, we focus on a column with the nominal feed flow rates $F_{B,1} = 5.5$ mol/s, $F_{A,4} = 5.775$ mol/s, and reboiler heat duty $Q_h = 5.5$ MW. Note that ethylene oxide (A) is fed in slight excess of water (B). The feed ratio should ideally be close to one to allow a high product purity $x_{C,N+1}$. However, a slight variation in one or both feeds has a strong influence on the dynamic behavior of the column. We will discuss this issue in further detail later in the control section. For the nominal column configuration, we investigate the possibility of multiple steady states through a homotopy continuation similar to Ciric and Miao (1994), where the reaction terms in the modeling equations are multiplied by a factor of λ. The variation in the steady-state product composition $x_{C,N+1}$ is traced as the homotopy parameter λ is increased from an initial value of zero (nonreactive column). The value of $\lambda = 1$ corresponds to the nominal reactive distillation column. Figure 3a shows the variation of $x_{C,N+1}$ at steady state with λ. The steady states that are stable are represented on a solid curve, while unstable ones are represented on a dashed curve; the stability of the steady states is studied on the basis of the eigenvalues of the linear approximation of the dynamic model.

Clearly, the reactive distillation column ($\lambda = 1$) has three distinct steady states. The low conversion steady state lies on the stable lower branch, which passes through a turning point at $\lambda = 3.81$, where one of the eigenvalues of the linearized system crosses over to the right of the imaginary axis. The medium conversion steady state lies on the middle branch which is unstable and passes through another turning point at $\lambda = 0.78$, where another eigenvalue crosses to the right. Finally, both the unstable eigenvalues become complex conjugate as they cross back to the left of the imaginary axis at a Hopf bifurcation point at $\lambda = 0.79$, indicating the possible existence of periodic solutions. The third steady state with a high conversion lies on the upper branch which is stable. While the existence of the three steady states at $\lambda = 1$ is in accordance with the results of Ciric and Miao (1994), there are several qualitative differences. For instance, the left turning point is far away from $\lambda = 0$ and the upper branch covers a much wider range of product purity, or equivalently, production rate of ethylene glycol (the product flow rate F_p given by Eq. 36 is constant along the upper branch since $x_{A,N+1} = 0$). These discrepancies can be ascribed to certain differences in the modeling assumptions and parameter values. For example, contrary to Ciric and Miao (1994), we do not assume that the reactions are constrained to occur only in the top section of the column, or that the liquid-phase specific enthalpies are negligible compared to the heats of reaction and the latent heat of vaporization, since the temperature variation is a key source of nonlinearity.

We also studied the effect of varying the feed flow rates and the reboiler heat input on the shape of the steady-state curve and the number of steady states. Figure 3b depicts the steady-state curves for the nominal reactant flow rates (I), reduced flow rates $F_{B,1} = 1.3$ mol/s, $F_{A,4} = 1.365$ mol/s (II), and higher flow rates $F_{B,1} = 10.0$ mol/s, $F_{A,4} = 10.5$ mol/s

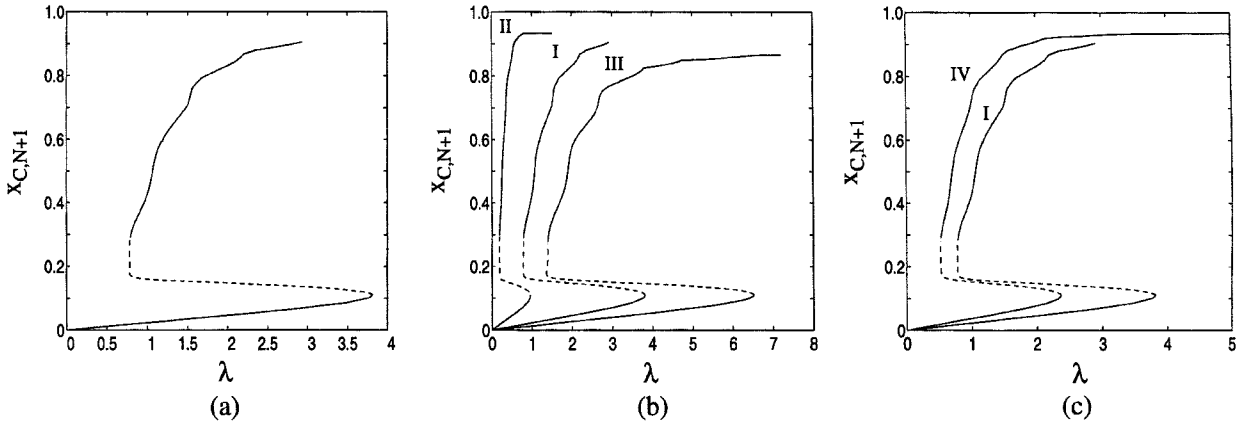

Figure 3. (a) Variation of steady-state product composition with λ (stable (——), unstable (– – –)), variation of steady-state curve with (b) reactant flow rates, and (c) heat input in reboiler.

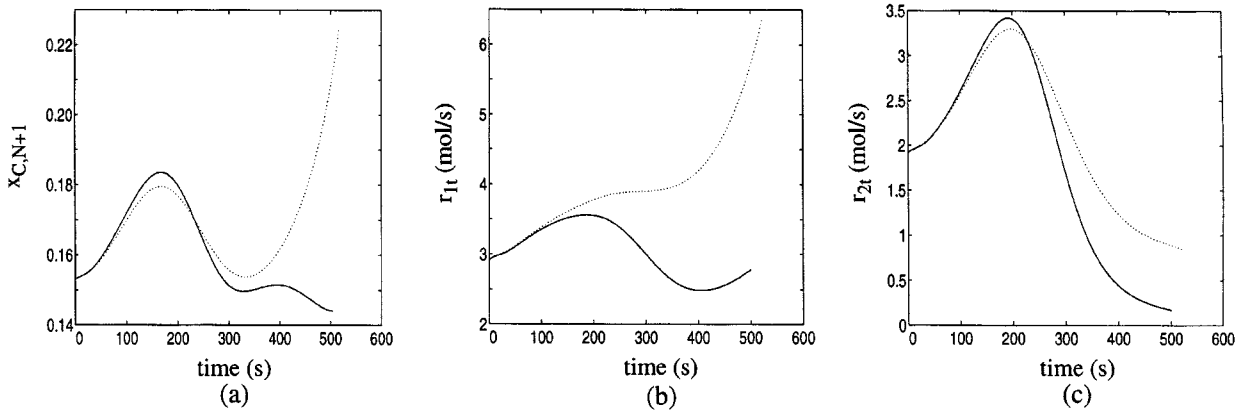

Figure 4. (a) Product composition; (b) total reaction rate for the main reaction; (c) total reaction rate for the side reaction, as predicted by the index-one (· · · ·) and index-two (——) DAE models.

(III); the feed ratio $F_{A,4}/F_{B,1}$ is kept constant at 1.05. Clearly, for the low reactant feed flow rates (case II), and, consequently, lower product flow rate F_p, the whole curve shifts to the left such that the right turning point is below $\lambda = 1$ and the column possesses a single high conversion steady state. On the other hand, for high feed flow rates (case III), the curve shifts to the right such that the left turning point is above $\lambda = 1$ and the column again possesses only a single low conversion steady state. Thus, as the reactant and product flow rates increase (decrease) compared to the internal liquid and vapor flow rates in the column, the conversion decreases (increases).

The variation of the steady-state curve with the heat input Q_h in the reboiler is shown in Figure 3c. Clearly, as the heat duty Q_h in the reboiler is increased to 7.0 MW (case IV), and, consequently, Q_c is also increased to maintain atmospheric pressure in the top tray, the internal liquid and vapor flow rates increase to yield a higher conversion, shifting the curve to the left.

Despite the fact that the index-one and index-two DAE models have the same *steady states*, the index-one model may predict a significantly different *dynamic behavior* of the process as compared to that predicted by the more detailed index-two model. To illustrate these differences, we performed dynamic simulations of the index-two DAE model (Eqs. 4 to 19) using a minimal-order state-space realization (see the section on control at moderate purity for a discussion on the state-space realization), and the simplified index-one DAE model (Eqs. 24 to 34). Figure 4 shows a comparison of the profiles for the product composition $x_{C,N+1}$ and the total (over all stages) reaction rates $r_{1t} = \sum_{i=1}^{8} r_{1,i}$ and $r_{2t} = \sum_{i=1}^{8} r_{2,i}$ predicted by the two models, starting from a steady state corresponding to medium conversion on the middle branch in case (IV) (see Figure 3c) and for an increased reactant feed flow rate $F_{B,1} = 15.5$ mol/s, increased product flow rate $F_p = 20.5$ mol/s, increased heat input $Q_h = 7.2$ MW and reduced heat removal $Q_c = 6.9$ MW (steady-state values of F_p and Q_c are 6.46 mol/s and 7.2 MW, respectively). Clearly, the index-one model predicts significantly higher reaction rates and production of C than the index-two model. This is consistent with the fact that the assumption of a negligible vapor holdup in the former model implies that *all* the reactants and the products reside in the liquid (reaction) phase, without any separation into the nonreactive vapor phase. These differences indicate that the detailed index-two model should be preferred over the index-one model for an accurate description of the dynamic behavior of the column, and the design of effective model-based controllers.

Control Studies

We address the control of the column with a nominal water feed $F_{B,1} = 5.5$ mol/s and a nominal ethylene oxide feed $F_{A,4} = 5.775$ mol/s. In the previous section, we studied the steady-state multiplicity in the column with perfect control of the top pressure P_1 and the reboiler liquid holdup M_{N+1}^{l}, using Q_c and F_p as the corresponding inputs. Besides controlling these two outputs, the primary objective is to control

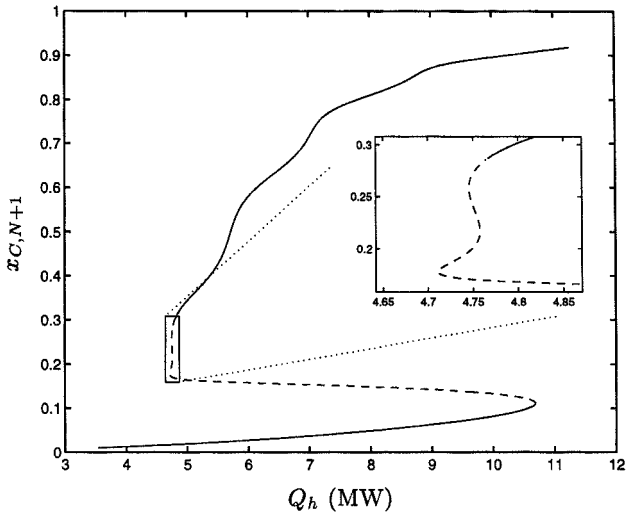

Figure 5. Variation of steady-state product purity $x_{C,N+1}$ with reboiler heat duty Q_h (stable (——), unstable (– – –)).

the product purity, that is, the mole fraction $x_{C,N+1}$, with the reboiler heat duty Q_h as the additional manipulated input.

Output multiplicity

In this section, we investigate the possibility of input and output multiplicities in the column with respect to the primary output $x_{C,N+1}$ and input Q_h. The same perfect controllers for P_1 and M^l_{N+1} were used to ensure that the overall material and energy balances in the column are satisfied as the reboiler heat input Q_h is varied. The plot for the steady-state variation of $x_{C,N+1}$ with Q_h is shown in Figure 5, where the stable and unstable steady states are indicated by solid and dashed lines, respectively. Clearly, the plot shows a three-branch output multiplicity, and in a small range of the input around $Q_h = 4.75$ MW, there exist up to five steady states.

Along the lower branch, for a low reboiler heat input $Q_h =$ 3.5 MW, the temperature in the column is too low for any significant reaction and the column essentially behaves as an ordinary nonreactive distillation column for water and ethylene oxide. As the heat input Q_h is increased, the temperature in the reboiler increases enough for the reactions to occur. Figure 6 shows the variation with Q_h in the composition, temperature, and reaction rate profiles and a comparison of the total (on all stages) reaction rates r_{1t} (solid) and r_{2t} (dashed) for the two reactions in Eq. 1 and Eq. 2, along the lower branch. Clearly, both the reaction rates increase simultaneously in the reboiler with increasing temperature and this lower branch corresponds to low conversion and low

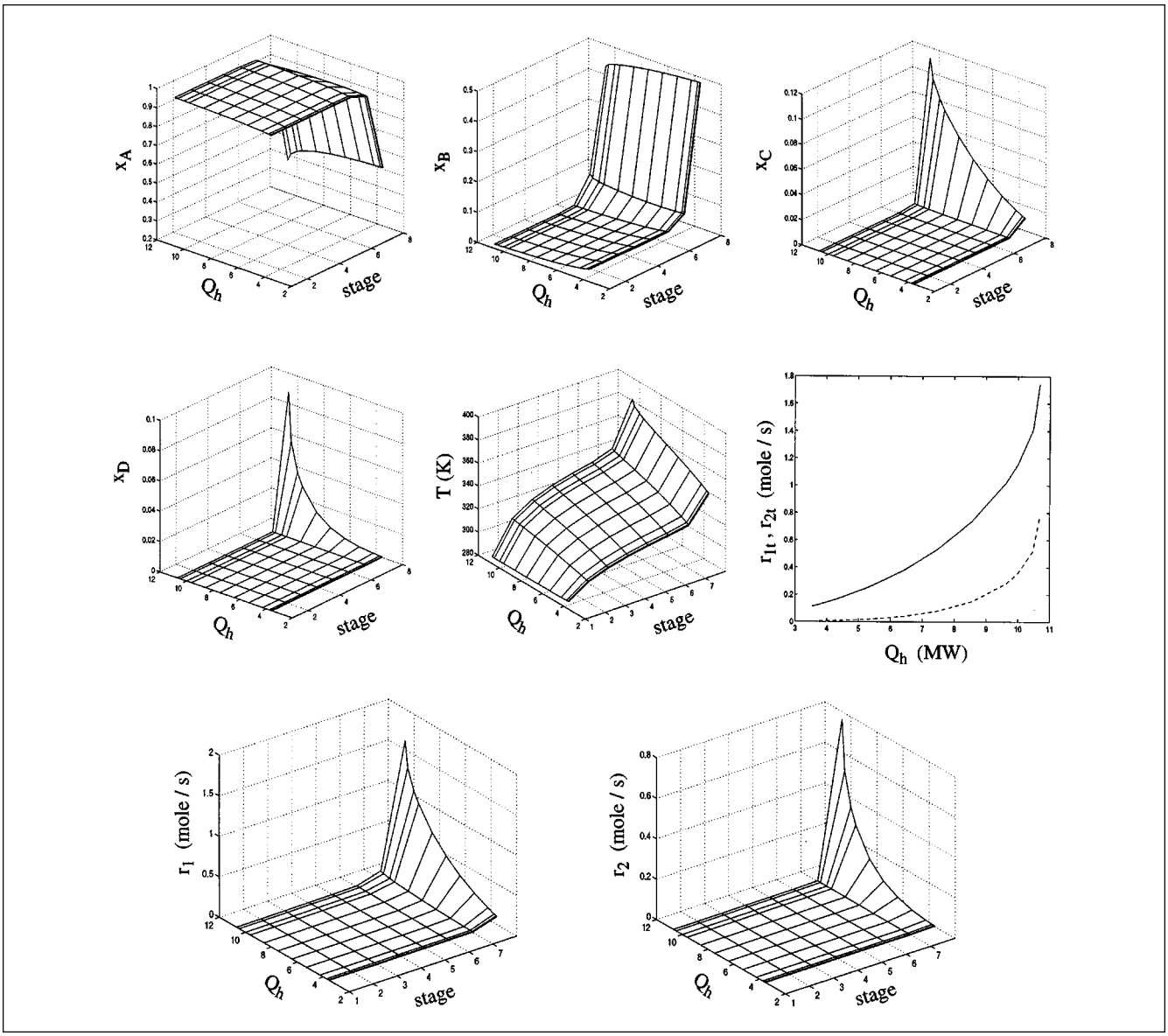

Figure 6. Variation in composition, temperature, and reaction profiles in the column with varying heat input Q_h along the lower steady-state branch.

product selectivity. The composition essentially changes only in the reboiler as ethylene glycol and diethylene glycol are produced.

Figure 7 shows the variation of the composition, temperature, and reaction profiles with Q_h along the middle branch. Clearly, the reactions are still confined essentially to the reboiler and proceed from a moderate to almost complete conversion of ethylene oxide ($x_{A,\,N+1} \rightarrow 0$). However, as more ethylene glycol is produced, it is consumed in the faster secondary reaction to yield the byproduct diethylene glycol. Thus, this middle branch corresponds to steady states with high conversion of ethylene oxide, low conversion of water, and, consequently, low product selectivity ($x_{D,\,N+1} > x_{C,\,N+1}$).

Figure 8 shows the composition, temperature and reaction profiles in the column along the upper branch of the bifurcation diagram. As the reboiler heat input is increased, the temperature in the column increases. Moreover, there is a significant amount of heavy products which displace the light reactants, ethylene oxide and water, from the reboiler into the column as Q_h is increased. These two effects together push the reaction zone upwards from the reboiler into the column (see the profile for r_1). Furthermore, owing to the large difference in the volatilities of ethylene oxide and water, the column begins to exhibit an excess of water compared to ethylene oxide in the reaction zone, thus favoring the main reaction in Eq. 1 while suppressing the formation of diethylene glycol in the side reaction (Eq. 2). So, this branch corresponds to complete conversion of ethylene oxide ($x_{A,\,N+1} \approx 0$), increasing conversion of water, and, hence, increasing product selectivity and purity.

It is desirable to operate the column at a steady state on the upper branch with high conversion and high selectivity. The three-branch output multiplicity clearly illustrates the nonlinear behavior of the column. Moreover, as we shall il-

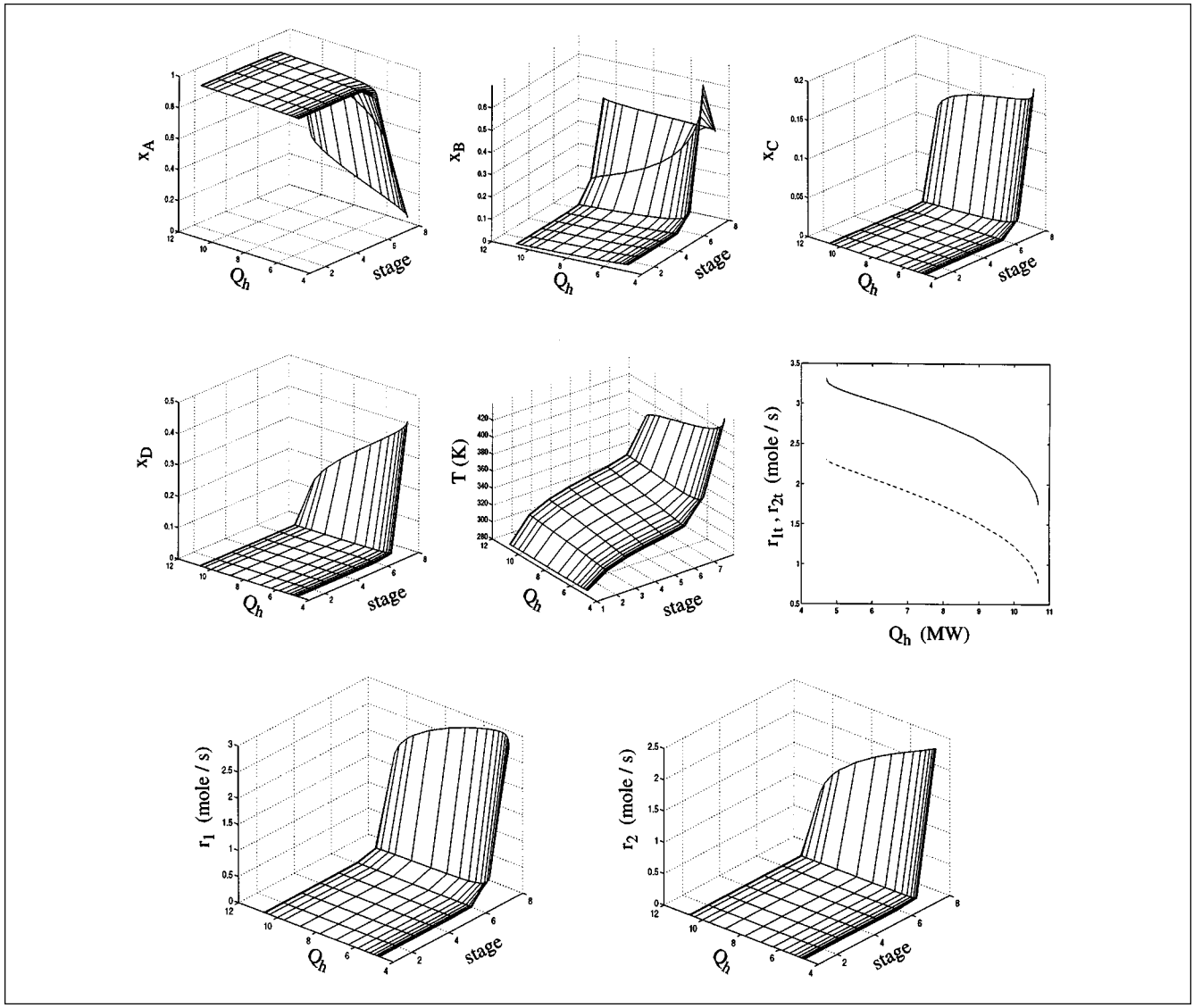

Figure 7. Variation in composition, temperature, and reaction profiles in the column with varying heat input Q_h along the middle steady-state branch.

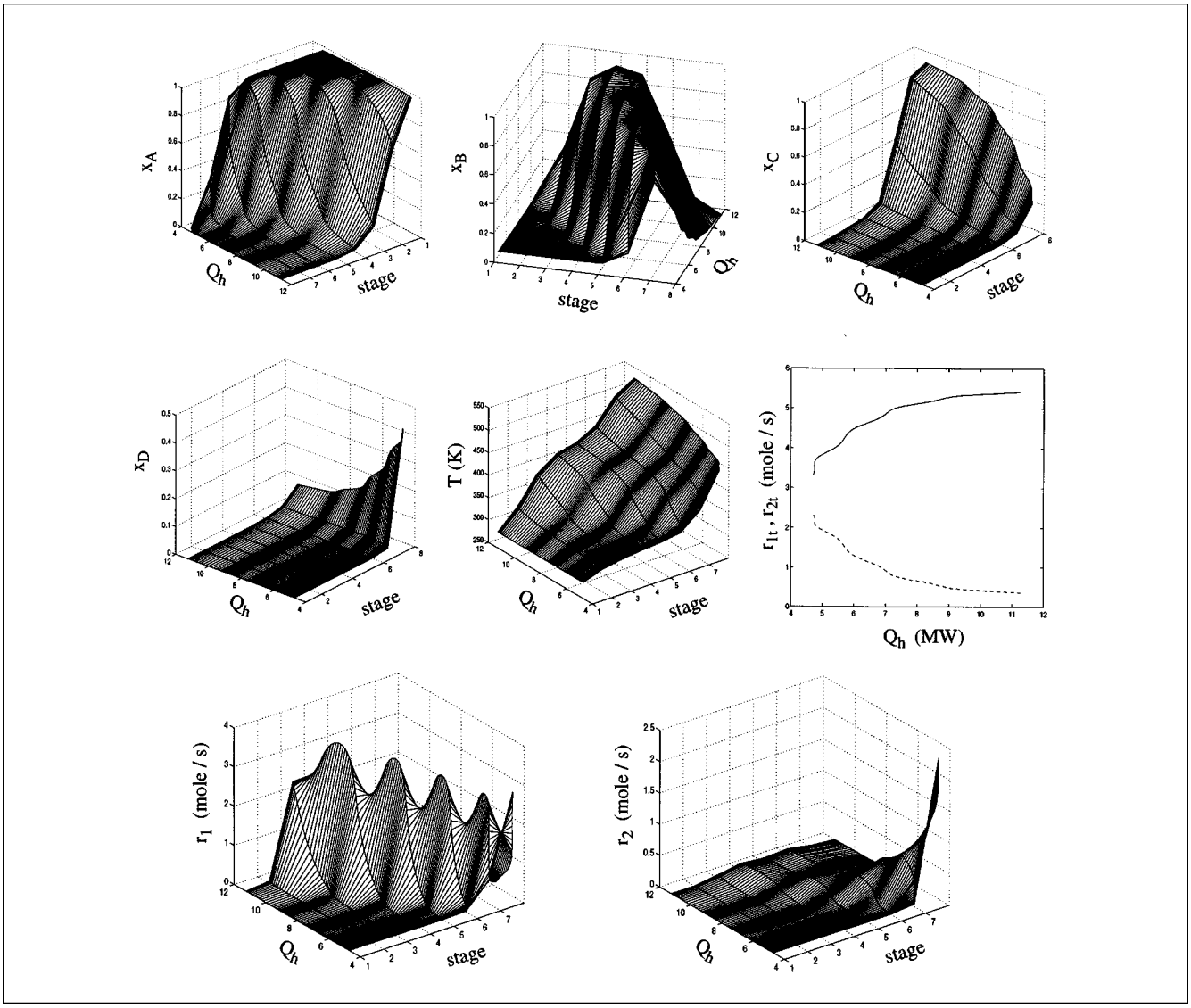

Figure 8. Variation in composition, temperature, and reaction profiles in the column with varying heat input Q_h along the upper steady-state branch.

lustrate in the next section, even along the upper steady-state branch, the column exhibits a fundamentally different behavior depending on the product purity.

High-purity column— Nonminimum phase behavior

We investigate the existence of nonminimum phase behavior in the column, along the upper steady-state branch of Figure 5. More specifically, we studied the location of the transmission zeros of a linear approximation of the state-space realization (see the next section) of the index-two DAE model. The study revealed a transition from a minimum phase behavior to a nonminimum phase behavior at $x_{C,N+1} = 0.814$. Figure 9 shows the upper steady-state branch where the steady states corresponding to minimum phase behavior are shown on a solid curve, while the ones corresponding to a nonminimum phase behavior are shown on a dashed curve. At moderate purity ($x_{C,N+1} < 0.814$), all zeros are to the left of the imaginary axis, that is, the system is minimum phase. At $x_{C,N+1} = 0.814$, a pair of complex conjugate zeros cross over to the right of the imaginary axis, while another pair of zeros cross to the right of the imaginary axis at $x_{C,N+1} = 0.8815$, and then back to the left at $x_{C,N+1} = 0.917$.

In what follows, we analyze the physical characteristics of the column along the upper steady-state branch to gain an insight into the transition from minimum phase behavior at moderate purity to a nonminimum phase behavior at high purity. Note first that at a steady state on this branch, the system is stable when only M^l_{N+1} and P_1 are controlled with F_p and Q_c, respectively, while $x_{C,N+1}$ is left uncontrolled (see Figure 5). This implies that, loosely speaking, the input-output pair (Q_h, $x_{C,N+1}$) is responsible for the nonminimum phase behavior. Furthermore, along this branch, $x_{C,N+1}$ increases with increasing reboiler heat input Q_h, which implies

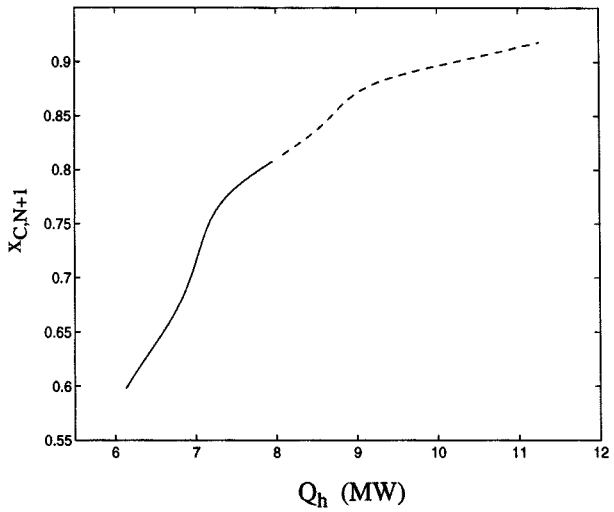

Figure 9. Steady states corresponding to minimum phase (——) and nonminimum phase behavior (– – –).

that the reaction in the column is always favorable for the product, in the sense that as Q_h increases, the conversion of water in the main reaction (Eq. 1), and, thus, the product selectivity increases, thereby increasing $x_{C,N+1}$. On the other hand, the distillation in the reboiler changes radically from moderate to high purity, and causes the transition from minimum phase to nonminimum phase behavior.

More specifically, at moderate purity, there is a significant amount of unconverted water at the bottom; Figure 10 shows the variation of the steady-state mole fraction of water in the reboiler $x_{B,N+1}$ with the heat input Q_h. The presence of water in the reboiler, which is lighter than ethylene glycol, ensures that the distillation in the reboiler is also favorable for the product; as the reboiler heat input Q_h is increased, water is preferentially vaporized and recycled in the vapor boilup, thereby increasing $x_{C,N+1}$.

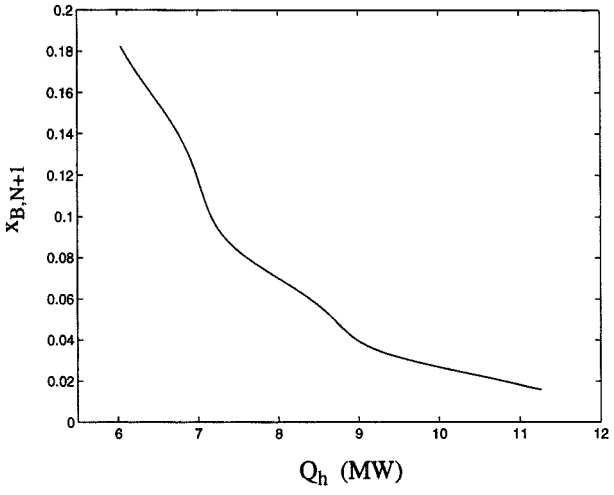

Figure 10. Steady-state variation of $x_{B,N+1}$ with Q_h along the upper branch.

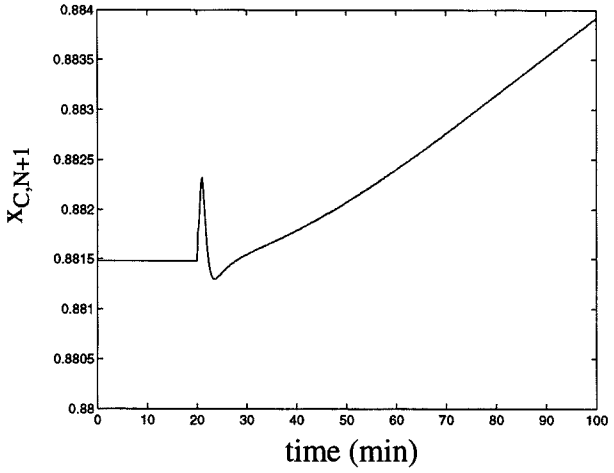

Figure 11. Response in $x_{C,N+1}$ for a step increase in Q_h under perfect control of P_1 and M^l_{N+1}.

However, in the high-purity region with a high $x_{C,N+1}$, water is almost completely consumed, that is, $x_{B,N+1} \approx 0$, and the liquid holdup in the reboiler essentially contains the product ethylene glycol and the byproduct diethylene glycol. Due to the absence of water in the reboiler, the distillation now favors the byproduct diethylene glycol, which is heavier than ethylene glycol; a higher heat input Q_h preferentially vaporizes and recycles ethylene glycol, thereby reducing $x_{C,N+1}$. A competition between the favorable reaction in the column that corresponds to a steady-state increase in $x_{C,N+1}$ with Q_h, and the *unfavorable* distillation in the reboiler that leads to a decrease in the transient response of $x_{C,N+1}$ for an increased Q_h, causes the nonminimum phase behavior. This is illustrated in Figure 11, which shows the response in $x_{C,N+1}$ for a 5% increase in Q_h, starting from a steady state with $x_{C,N+1} = 0.8815$ and under perfect control of P_1 and M^l_{N+1}. Note the inverse response in $x_{C,N+1}$ after an initial increase.

The nonminimum phase behavior in the high-purity region ($x_{C,N+1} > 0.814$) has serious consequences on the stability and performance characteristics of standard linear and nonlinear controllers. We will illustrate these limitations later, and address the design of a nonlinear controller that yields a good set point tracking performance with closed-loop stability.

Control at moderate purity

In this section, we address the control of the seven-tray column in the moderate purity region ($x_{C,N+1} < 0.814$). More specifically, for the process where it is desired to control the outputs $y_1 = x_{C,N+1}$, $y_2 = M^l_{N+1}$ and $y_3 = P_1$, using the manipulated inputs $u_1 = Q_h$, $u_2 = F_p$ and $u_3 = Q_c$, we will design a nonlinear controller on the basis of the index-two DAE model in Eqs. 4 to 19.

A systematic framework for the design of feedback controllers for nonlinear high-index DAE systems was developed in Kumar and Daoutidis (1995c). More specifically, DAE systems with the following general description were considered

$$\dot{x} = f(x) + b(x)z + g(x)u$$

$$0 = k(x) + l(x)z$$

$$y_i = h_i(x), \quad i = 1, \ldots, m \tag{37}$$

where $x \in \mathfrak{X} \subset \mathbb{R}^n$ is the vector of differential variables for which we have explicit differential equations, $z \in \mathfrak{Z} \subset \mathbb{R}^p$ is the vector of algebraic variables which evolve according to the algebraic equations, $u \in \mathbb{R}^m$ is the vector of manipulated inputs and y_i are the outputs to be controlled. The controller design for the DAE system in Eq. 37 entailed the derivation of a state-space realization, which was addressed through an algorithmic procedure involving a systematic identification of the underlying constraints in x imposed by the singular algebraic equations and the differentiation of these constraints to obtain a solution for z.

For the index-two DAE model of the column, the differential variables for each stage i are $x^i = [M_i^v \; y_{A,i} \; y_{B,i} \; y_{C,i} \; M_i^l \; x_{A,i} \; x_{B,i} \; x_{C,i} \; T_i]^T$ while the algebraic variables are $z^i = [N_{A,i} \; N_{B,i} \; N_{C,i} \; N_{D,i} \; P_i \; L_i \; V_i]^T$, except in stages 1 and $N+1$ where there is no pressure drop correlation and Francis weir formula, respectively, and the algebraic variables do not include V_1 and L_{N+1}. Note, however, that for the stages $i = 2, \ldots, N+1$, the vapor flow rate V_i appears in a nonlinear fashion in the pressure drop correlation (Eq. 18). Thus, in order to obtain a DAE model in the form of Eq. 37 that is linear (affine) in the algebraic variables z, the vapor flow rate V_i for these stages is included in an extended vector of differential variables $\hat{x}^i = [x^{i^T} \; V_i]^T$, and its time-derivative $\overline{V}_i = \dot{V}_i$ is included in the vector algebraic variables (for more details, see Kumar and Daoutidis, 1995a).

The resulting DAE system has altogether $n = 10(N+1) - 1$ differential variables, $p = 7(N+1) - 2$ algebraic variables, and $m = 3$ outputs and manipulated inputs, and the algorithmic procedure of Kumar and Daoutidis (1995c) converges in one iteration. More specifically, for each stage i, the singular algebraic equations (Eq. 13 to Eq. 19) impose five constraints in the differential variables $\hat{x}^i$. These constraints are easily obtained by solving for P_i in terms of $\hat{x}^i$ from the ideal gas equation (Eq. 17), and substituting the solution in phase equilibrium relations (Eq. 13 to Eq. 16) and the pressure drop correlation (Eq. 18). The resulting constraints are

$$k^{i,1}(\hat{x}) = \begin{bmatrix} \dfrac{\rho_i^l M_i^v R T_i y_{A,i}}{\rho_i^l V_t - M_i^l} - P_{A,i}^s x_{A,i} \\ \dfrac{\rho_i^l M_i^v R T_i y_{B,i}}{\rho_i^l V_t - M_i^l} - P_{B,i}^s x_{B,i} \\ \dfrac{\rho_i^l M_i^v R T_i y_{C,i}}{\rho_i^l V_t - M_i^l} - P_{C,i}^s x_{C,i} \\ \dfrac{\rho_i^l M_i^v R T_i y_{D,i}}{\rho_i^l V_t - M_i^l} - P_{D,i}^s x_{D,i} \\ \dfrac{\rho_i^l M_i^v R T_i}{\rho_i^l V_t - M_i^l} - \dfrac{\rho_{i-1}^l M_{i-1}^v R T_{i-1}}{\rho_{i-1}^l V_t - M_{i-1}^l} - \sigma_1\left(\dfrac{V_i(\rho_i^l V_t - M_i^l)}{\rho_i^l M_i^v}\right)^2 - \sigma_2\left(\dfrac{M_{i-1}^l}{\rho_{i-1}^l}\right) \end{bmatrix} = 0 \tag{38}$$

Differentiating these constraints once, the resulting algebraic equations can be solved for $N_{A,i}$, $N_{B,i}$, $N_{C,i}$, $N_{D,i}$ and $\overline{V}_i$, implying that index is $\nu_d = 2$. Thus, a state-space realization of the DAE model on the constrained state space specified by the constraints in Eq. 38 can be obtained by substituting the solution for the algebraic variables in the differential equations. Furthermore, the above constraints $k^{i,1}(\hat{x})$ in Eq. 38 can also be used in the coordinate change (for further details, see Kumar and Daoutidis, 1995c)

$$\zeta^i = \begin{bmatrix} \zeta_1^{i,0} \\ \zeta_2^{i,0} \\ \zeta_3^{i,0} \\ \zeta_4^{i,0} \\ \zeta_5^{i,0} \\ \zeta^{i,1} \end{bmatrix} = \begin{bmatrix} M_i^l \\ x_{A,i} \\ x_{B,i} \\ x_{C,i} \\ T_i \\ k^{i,1}(\hat{x}) \end{bmatrix} \tag{39}$$

to obtain a minimal-order state-space realization of dimension $5(N+1)$ with exactly the same states $\zeta^{i,0} = [M_i^l \; x_{A,i} \; x_{B,i} \; x_{C,i} \; T_i]^T$ as in the index-one DAE model with negligible vapor holdup assumption (Eqs. 24 to 34). For this minimal-order state-space realization, the relative orders of the three outputs with respect to the manipulated input vector u are $r_1 = 1$, $r_2 = 1$, and $r_3 = 1$, and the characteristic matrix is nonsingular.

An input/output linearizing controller was designed on the basis of the minimal-order state-space realization of the index-two model to enforce the following decoupled first-order responses in the closed-loop system

$$y_i + \gamma_i \frac{dy_i}{dt} = y_{isp}, \quad i = 1, 2, 3 \tag{40}$$

where y_{isp} is the set point for the output y_i, and γ_1, γ_2 and γ_3 are adjustable scalar parameters. Figure 12 shows the performance of the controller in the nominal process for a 5% increase in the set point for product purity y_{sp1} starting at a nominal steady state with $x_{C,N+1} = 0.748$. The controller was tuned with the parameters $\gamma_1 = 3.33$ h, $\gamma_2 = 1.67$ h, and $\gamma_3 = 0.83$ h. Clearly, the controller enforces the requested linear response, and the manipulated inputs also vary smoothly to their respective steady-state values.

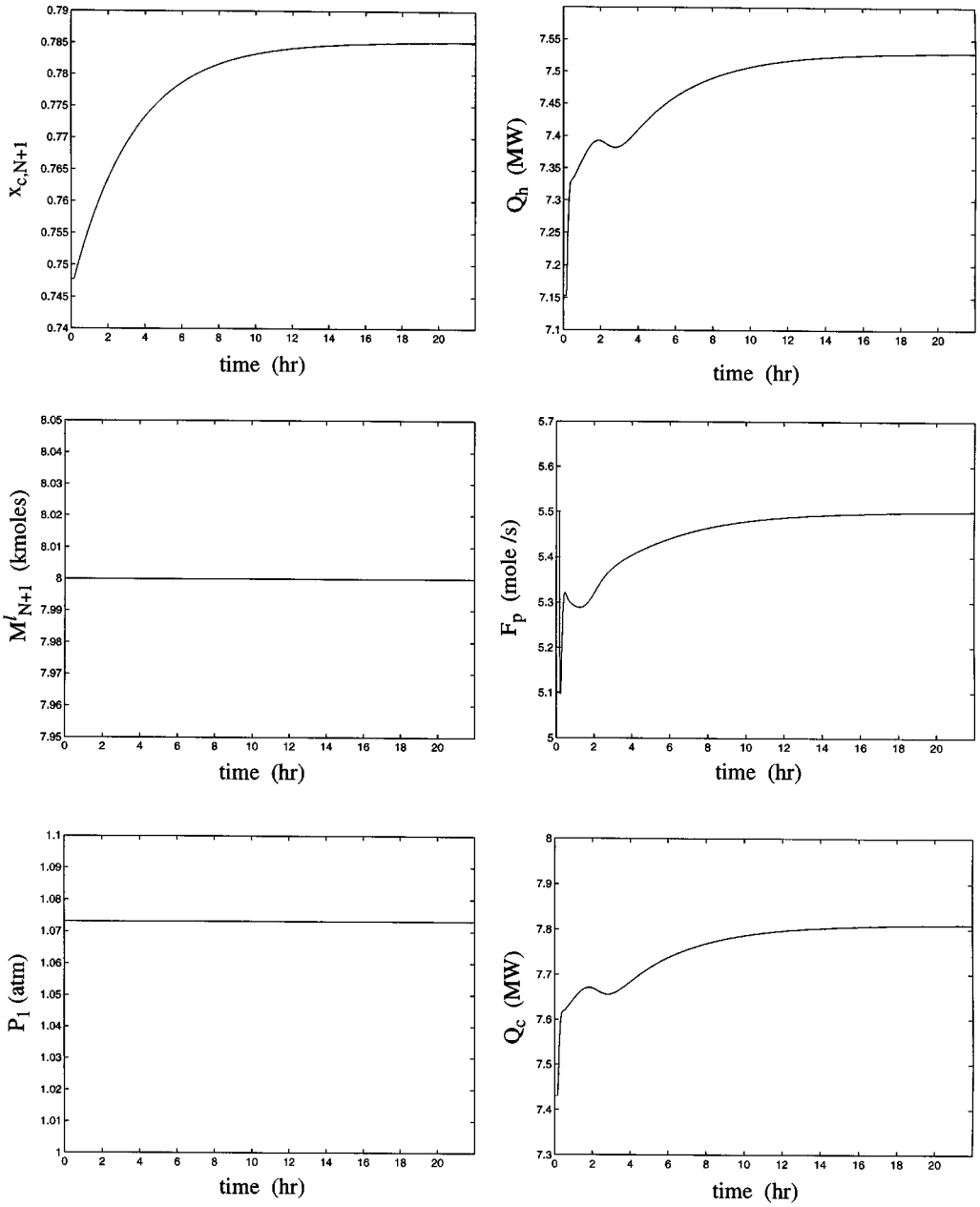

Figure 12. Closed-loop profiles under input/output linearizing controller at moderate purity for a 5% step increase in the set point for $x_{C,N+1}$.

Control at high purity

Unlike in the moderate purity region, the input/output linearizing controller designed to enforce the response in Eq. 40 leads to closed-loop instability in the high-purity region. Figure 13 shows the closed-loop input and output profiles under the controller, starting at an initial condition $x(0)$ perturbed slightly from the steady state corresponding to $x_{C,N+1} = 0.8815$. Clearly, the closed-loop system is unstable, which corroborates the observation of nonminimum phase behavior on the basis of the zeros of the linearized model discussed earlier.

We also studied the performance of PI controllers designed to control the top pressure P_1 with Q_c, the reboiler liquid holdup M^l_{N+1} with F_p and the product composition $x_{C,N+1}$ with Q_h, through simulations in this high-purity region. The three PI controllers

$$Q_h = Q_{h,\text{nom}} + K_{c1}\left(y_{1sp} - x_{C,N+1} + \frac{1}{t_{I1}}\int_0^t \left(y_{1sp} - x_{C,N+1}(\tau)\right) d\tau \right)$$

$$F_p = F_{p,\text{nom}} + K_{c2}\left(y_{2sp} - M^l_{N+1} + \frac{1}{t_{I2}}\int_0^t \left(y_{2sp} - M^l_{N+1}(\tau)\right) d\tau \right)$$

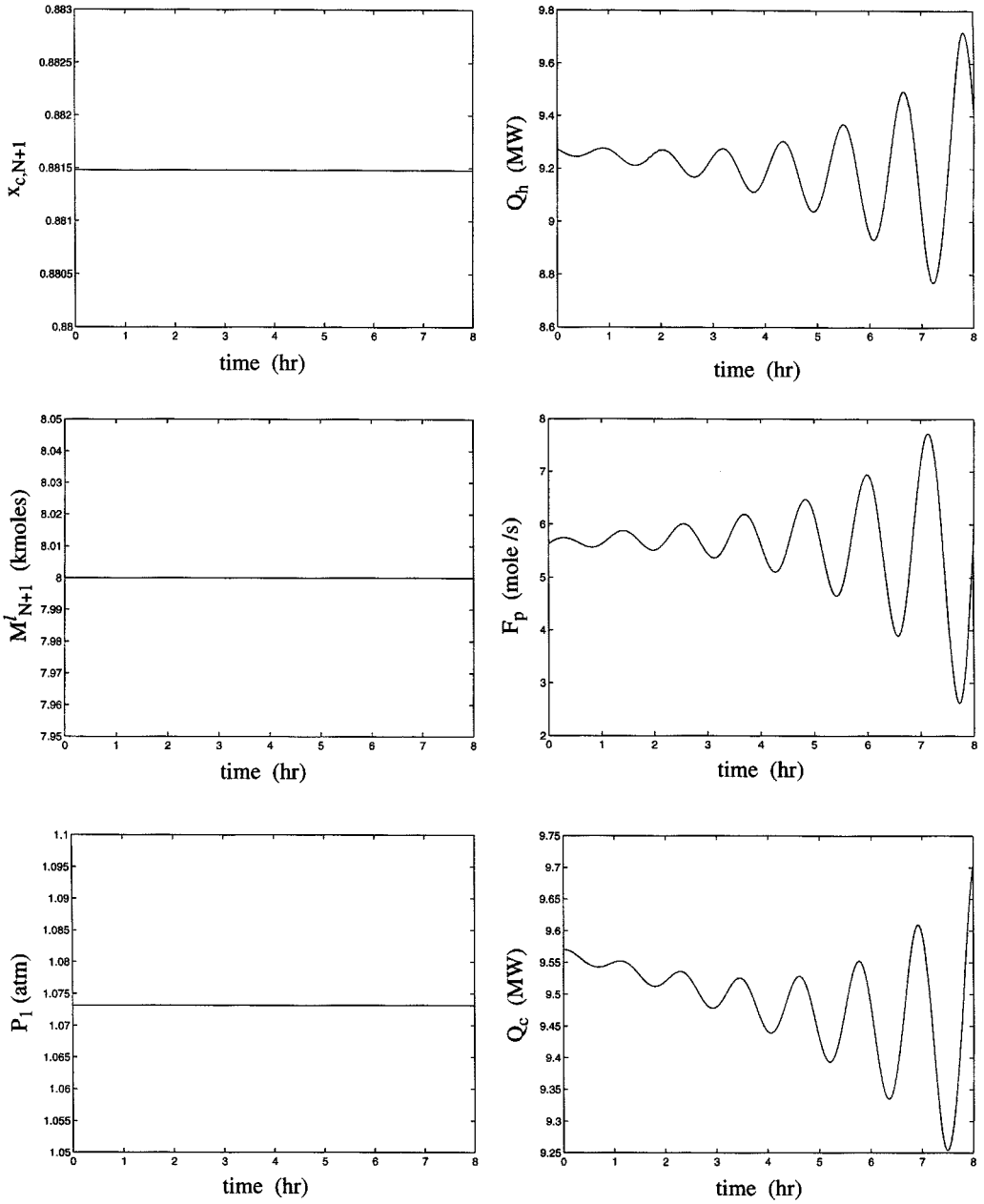

Figure 13. Closed-loop profiles under input/output linearizing controller at high purity.

$$Q_c = Q_{c,\text{nom}} + K_{c3}\left(y_{3sp} - P_1 + \frac{1}{t_{I3}}\int_0^t \left(y_{3sp} - P_1(\tau)\right) d\tau \right) \quad (41)$$

where nom refers to the nominal steady-state values of the respective inputs, were tuned with the following parameters

$$\begin{aligned} K_{c1} &= 3.0 \text{ MW/mol \%}, & t_{I1} &= 0.556 \text{ min} \\ K_{c2} &= -2.0 \text{ mol/s}\cdot\text{kmol}, & t_{I2} &= 1.67 \text{ min} \\ K_{c3} &= -0.5 \text{ MW/atm}, & t_{I3} &= 1.67 \text{ min} \end{aligned} \quad (42)$$

Figure 14 shows the performance of the PI controllers for a 5% increase in the set point y_{1sp} for product purity starting from the nominal steady state at $x_{C,N+1} = 0.8815$ and three different values of the controller gain K_{c1}. The controller with a low gain $K_{c1} = 3.0$ yields a smooth but very slow response. For a higher gain $K_{c1} = 5.0$, the controller performs slightly better (in terms of reaching the new set point faster), albeit with some overshoot. As the gain is increased to $K_{c1} = 7.0$, the controller calculates large heat duties in the reboiler and condenser and the performance deteriorates significantly. A further increase in the gain leads to an instability due to the nonminimum phase behavior.

The simulations with the input/output linearizing controller and the PI controllers demonstrate the need for a nonlinear controller that accounts for the nonminimum phase

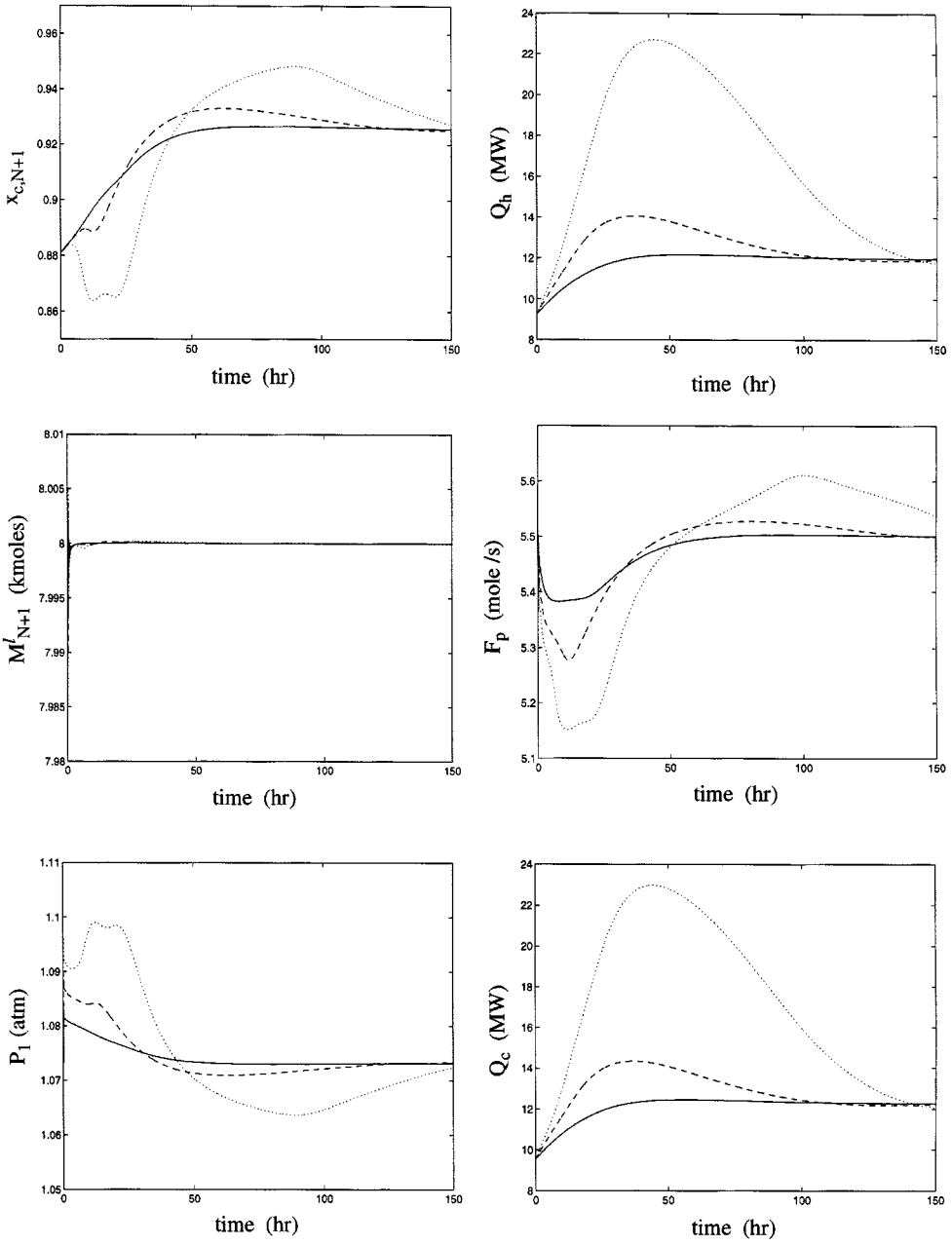

Figure 14. Closed-loop profiles with PI controllers at high purity, with different controller gains $K_{c1} = 3$ (——), $K_{c1} = 5$ (– – –), and $K_{c1} = 7$ (· · · ·).

behavior of the column at high purity and yields an improved performance with closed-loop stability. In the rest of this section, we will address the design of such a controller.

The control of nonlinear nonminimum phase systems is a challenging problem and an active area of research. A general and practical controller design method that addresses both stability and performance issues in nonlinear nonminimum phase systems is not available. One approach is to design a nonlinear regulator (Isidori and Byrnes, 1990) whose stability characteristics are independent of whether the process is minimum phase or not. However, the application of this approach is limited by the fact that the controller design involves the highly difficult task of solving a set of nonlinear partial differential equations. On the other hand, standard inversion-based controllers lead to closed-loop instability for nonminimum phase systems. In light of this problem, specific controller design methods have been proposed for some limited classes of nonlinear systems. More specifically, the control of second-order nonlinear nonminimum phase systems has been addressed in Kravaris and Daoutidis (1990), while for higher-order nonlinear SISO systems that are completely state-space linearizable, an approach based on the calculation of a ''statically equivalent'' output with respect to which the system is minimum phase was proposed in Wright and Kravaris (1992). In a similar vein, for a class of nonlinear maximum phase SISO systems, that is, systems with no stable

or center manifolds in the zero dynamics, an approach for approximate linearization was proposed in Doyle III et al. (1996), which involves a modification of the input and its derivatives, rather than the output, in an observability canonical form representation of the system.

We address the controller design for the high-purity column following the approach of statically equivalent outputs. To this end, we will construct an auxiliary output $\tilde{y}_1$ such that: (i) $\tilde{y}_1$ is statically equivalent to the process output y_1, that is, $\tilde{y}_1 = y_1$ at every steady state, and (ii) the system is minimum phase with respect to $\tilde{y}_1$ (and the other outputs y_2, y_3). Once such an output $\tilde{y}_1$ is constructed, an input/output linearizing controller designed for $\tilde{y}_1$ will yield asymptotic tracking for y_1 with closed-loop stability. Note that the choice of such a statically equivalent output is not unique, but it affects the transient performance of the controller. The design of a statically equivalent output that yields good control performance was addressed in Wright and Kravaris (1992) through an ISE optimization problem. However, the solution of such an optimization problem is difficult for general nonlinear systems and analytical solutions are available only for the specific class of nth order systems with a relative order $r = n - 1$ (Wright and Kravaris, 1992). In what follows, we propose a statically equivalent output $\tilde{y}_1$ for the column such that the resulting controller yields good performance with stability.

Consider an output of the form

$$\tilde{y}_1 = x_{C,\,N+1} + \gamma_1 \frac{dx_{C,\,N+1}}{dt} + \alpha\left(\zeta^{(0)},\, u\right) \tag{43}$$

where $\zeta^{(0)}$ is the state vector for the minimal-order state-space realization of the index-two DAE model, γ_1 is a scalar parameter, $(dx_{C,\,N+1}/dt)$ is given by the differential equation for $x_{C,\,N+1}$ in the index-two model, and the term α is to be designed. The above form for $\tilde{y}_1$ is motivated by several factors. First, note that the term $x_{C,\,N+1} + \gamma_1(dx_{C,\,N+1}/dt)$ is statically equivalent to y_1 and it corresponds to the usual first-order linear response in y_1 requested in the standard input/output linearization, that is, for $\alpha \equiv 0$, a controller designed to enforce $\tilde{y}_1 = y_{1sp}$ (the relative order of $\tilde{y}_1$ is $\tilde{r}_1 = 0$) essentially induces a first-order linear response in y_1. Clearly, such a controller would lead to closed-loop instability. The term α is a design parameter that will allow overcoming this limitation of the input/output linearizing controller. In particular, α will be designed such that (i) the system with the output $\tilde{y}_1$ is minimum phase and a controller that enforces $\tilde{y}_1 = y_{1sp}$ does so with closed-loop stability, and (ii) at any steady state $(\zeta_s^{(0)},\, u_s)$, $\alpha(\zeta_s^{(0)},\, u_s) = 0$ so that $\tilde{y}_1$ is statically equivalent to y_1. Recently, a similar approach for designing a statically equivalent output for nonlinear nonminimum phase systems has been proposed in Kravaris et al. (1997), where a linear combination of the process output and the time-derivatives of the states is considered as a choice for the statically equivalent output.

With the above observations, we address the design of α by focusing on modifying the destabilizing effect of the unfavorable distillation in the reboiler. More specifically, consider the column with the feed ratio

$$\frac{F_{A,4}}{F_{B,1}} = 1 + r_F \tag{44}$$

where $r_F = 0$, $r_F > 0$ and $r_F < 0$ correspond to a stoichiometric feed ratio (with respect to the main reaction in Eq. 1), excess A, and excess B, respectively. The steady-state overall material balances for the conversion of ethylene oxide (A) and water (B) in the column, yield the following relations

$$F_{A,4} - F_p x_{A,\,N+1s} = F_p x_{C,\,N+1s} + 2F_p x_{D,\,N+1s}$$

$$F_p = \frac{F_{B,1}}{1 - x_{A,\,N+1s}} \tag{45}$$

In the high-purity region, ethylene oxide is completely consumed in the two reactions, that is, $x_{A,\,N+1s} = 0$. Thus, $F_p = F_{B,1}$ and

$$x_{B,\,N+1s} = 0.5(1 - r_F - x_{C,\,N+1s}),$$
$$x_{D,\,N+1s} = 0.5(1 + r_F - x_{C,\,N+1s}) \tag{46}$$

Note that for a fixed feed ratio r_F, the steady-state product composition $x_{C,\,N+1s}$ increases with Q_h (Figure 5), and, thus, from Eq. 46, $x_{B,\,N+1s}$ and $x_{D,\,N+1s}$ decrease with Q_h. However, the difference $x_{D,\,N+1s} - x_{B,\,N+1s} = r_F$ is constant and depends only on the feed ratio. On the other hand, starting from a steady state, as Q_h is increased, $x_{B,\,N+1}(t)$ decreases with time. Furthermore, at moderate purity, the favorable distillation yields an increasing $x_{C,\,N+1}(t)$. Thus, $x_{D,\,N+1}(t) = 1 - x_{B,\,N+1}(t) - x_{C,\,N+1}(t)$ initially increases slightly and then decreases so that $x_{D,\,N+1}(t) - x_{B,\,N+1}(t)$ stabilizes at the steady-state value r_F. In contrast, at high purity, owing to the unfavorable distillation, $x_{C,\,N+1}(t)$ also decreases after a slight initial increase. Thus, $x_{D,\,N+1}(t)$, and, consequently, the difference $x_{D,\,N+1}(t) - x_{B,\,N+1}(t)$ increases substantially from the steady-state value of r_F and needs to be stabilized.

Motivated by the above observations, we consider the following output

$$\tilde{y}_1 = \left[x_{C,\,N+1} + \gamma_1 \frac{dx_{C,\,N+1}}{dt} \right] + \beta \left[x_{D,\,N+1} - x_{B,\,N+1} + \hat{\gamma}_1 \frac{d\left(x_{D,\,N+1} - x_{B,\,N+1}\right)}{dt} - r_F \right] \tag{47}$$

where $\alpha = \beta[(x_{D,\,N+1} - x_{B,\,N+1}) + \hat{\gamma}_1(d(x_{D,\,N+1} - x_{B,\,N+1})/dt) - r_F]$ corresponds to the stabilization of $(x_{D,\,N+1} - x_{B,\,N+1})$ at its steady-state value r_F. Note that α is trivially zero at steady state, that is, $\tilde{y}_1$ in Eq. 47 is statically equivalent to y_1. With this new output $\tilde{y}_1$, a controller was designed to enforce the closed-loop response

$$\tilde{y}_1 = y_{1sp} \tag{48}$$

$$y_i + \gamma_i \frac{dy_i}{dt} = y_{1sp}, \quad i = 2, 3 \tag{49}$$

and its performance was studied through simulations.

The stability and performance characteristics of the controller depend on the adjustable parameters, especially the parameters β, γ_1, and $\hat{\gamma}_1$ in the definition of the output $\tilde{y}_1$ in Eq. 47. While γ_1 corresponds to the time constant of the first-order response for $x_{C,N+1}$ in a standard input/output linearization, $\hat{\gamma}_1$ corresponds to the time constant for the stabilization of $(x_{D,N+1} - x_{B,N+1})$ at its steady-state value r_F. The parameter β is the relative "weight" for the stabilization of $(x_{D,N+1} - x_{B,N+1})$. For $\beta = 0$, the controller reduces to the standard input/output linearizing controller designed to enforce a first-order linear response for $x_{C,N+1}$, which, however, leads to closed-loop instability. On the other hand, for $\beta = 1$ and $\hat{\gamma}_1 = \gamma_1$, it can be verified that

$$\tilde{y}_1 = (1 - 2x_{B,N+1}) - 2\gamma_1 \frac{dx_{B,N+1}}{dt} - r_F$$

and, thus, the controller reduces to an input/output linearizing controller for the output $x_{B,N+1}$, that is, the mole fraction of water, and enforces the following response

$$x_{B,N+1} + \gamma_1 \frac{dx_{B,N+1}}{dt} = 0.5(1 - r_F - y_{1sp})$$

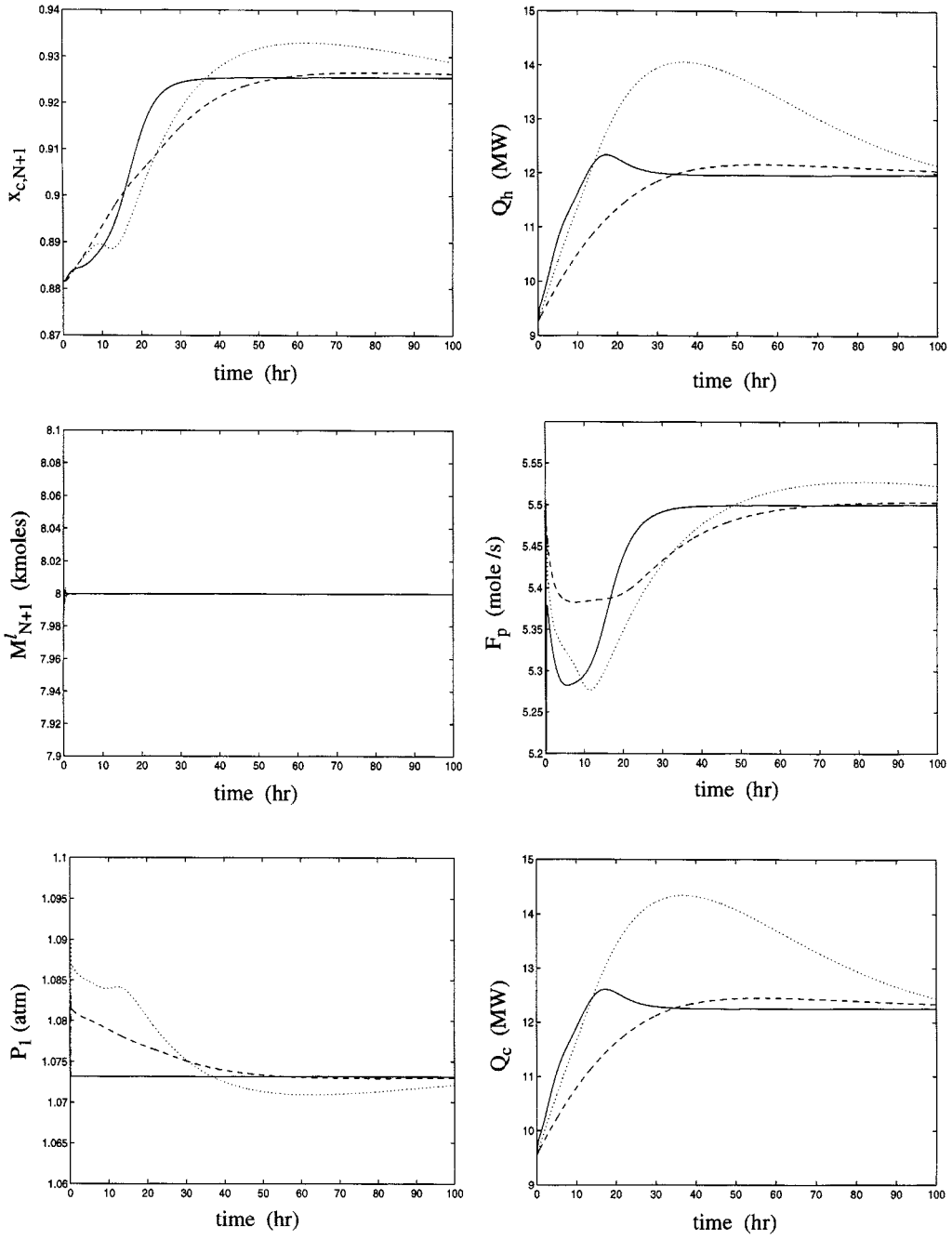

Figure 15. Closed-loop profiles for a 5% increase in y_{1sp} in high-purity region under proposed nonlinear controller (——), and PI controllers with $K_{c1} = 3.0$ (– – –), $K_{c1} = 5.0$ (· · · ·).

The process is minimum phase with respect to the output $x_{B,N+1}$, since both the reaction in the column, and the distillation in the reboiler are unfavorable for water, that is, an increase in Q_h leads to a decrease in $x_{B,N+1}$ in the transient response, as well as at steady state. Thus, for $\gamma_1 > 0$, this controller ensures closed-loop stability. Moreover, by regulating $x_{B,N+1}$ to the set point, $0.5(1 - r_F - y_{1sp})$, which corresponds to $x_{C,N+1} = y_{1sp}$ at steady state (see Eq. 46), the controller yields asymptotic tracking for the product purity $x_{C,N+1}$. However, its transient performance is not good, since $x_{C,N+1}$ is left uncontrolled and reaches the set point y_{1sp} very slowly. Given these two limiting cases, the parameters β, γ_1, and $\hat{\gamma}_1$ can be tuned to achieve optimum performance with closed-loop stability.

The controller was tuned with the parameters $\beta = 0.7$, $\gamma_1 = 2.0$ h, $\hat{\gamma}_1 = 3.6$ h, $\gamma_2 = 0.33$ h, and $\gamma_3 = 0.5$ h, and the closed-loop profiles for a 5% increase in y_{1sp} are compared with that of the PI controllers in Figure 15. Clearly, the proposed nonlinear controller yields a faster response in the product purity $x_{C,N+1}$ with no overshoot while maintaining y_2 and y_3 at the respective set points. Moreover, the calculated heat duties in the reboiler and the condenser also rise quickly from the initial nominal values to the final steady-state values. In contrast, the PI controller with $K_{c1} = 5$ evaluates large heat duties in the reboiler and condenser.

Remark 1. Until now, we focused on the column with a slight excess of ethylene oxide feed, $r_F = 0.05$. In this case, as water is completely consumed in the main reaction (Eq. 1), the excess ethylene oxide reacts with the product ethylene glycol in the side reaction (Eq. 2) to produce the heavier byproduct, diethylene glycol. Thus, as Q_h increases in the high-purity region, $x_{C,N+1s} \to (1 - r_F)$, and from Eq. 46, $x_{B,N+1s} \to 0$ and $x_{D,N+1s} \to r_F > 0$. The absence of (light) water, and the presence of the (heavy) byproduct diethylene glycol lead to the unfavorable distillation and, consequently, the nonminimum phase behavior. On the other hand, if water is fed in excess, that is, $r_F < 0$, then at high purity, all ethylene oxide is consumed primarily in the main reaction, with very little production of diethylene glycol in the side reaction. In particular, as Q_h increases, $x_{C,N+1s} \to (1 + r_F)$, and from Eq. 46, $x_{B,N+1s} \to -r_F > 0$ while $x_{D,N+1s} \to 0$. The presence of unconverted excess water in the reboiler ensures that the distillation is always favorable and the system is minimum phase. These obervations may suggest that the column should preferably be operated with excess water feed, close to the stoichiometric ratio, that is, $r_F = -\epsilon < 0$ (the maximum attainable purity is limited by $x_{C,N+1s} \le 1 - |r_F|$). However, this is not desirable from energy considerations. Figure 16 shows a comparison of the steady-state variation of $x_{C,N+1}$ with Q_h for $r_F = 0.05$ and $r_F = -0.045$. Clearly, in the case of excess water feed ($r_F = -0.045$), a much higher heat input Q_h is required to attain high product purity $x_{C,N+1}$. Furthermore, even if the nominal water feed is in slight excess over the nominal ethylene oxide feed, a slight change in one or both feed flow rates can easily lead to excess ethylene oxide and nonminimum phase behavior. Thus, the need for addressing the nonminimum phase behavior in the controller design cannot be avoided by modifying the column operation to excess water feed.

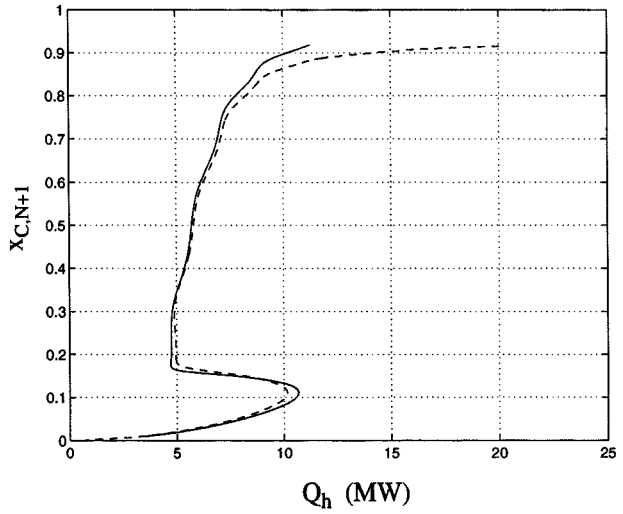

Figure 16. Steady-state variation of $x_{C,N+1}$ with Q_h for $r_F = 0.05$ (——) and $r_F = -0.045$ (– – –).

Conclusions

In this article, we addressed the dynamic modeling and control of an ethylene glycol reactive distillation column. We derived a detailed tray-by-tray model that includes the vapor-phase dynamic balances. A comparison of the dynamic behavior predicted by this model with that of a conventional model that ignores the vapor holdup illustrated the importance of including the vapor phase for an accurate description of the process dynamics. A steady-state bifurcation analysis for the column yielded the existence of up to five steady states, indicating the presence of strong nonlinearities even in the case of ideal phase behavior. Moreover, the column was found to exhibit a nonminimum phase behavior at high purity, which makes the design of effective controllers a challenging problem. A nonlinear controller that yields good performance with stability in the high-purity region was developed with the aid of a physical insight into the nonminimum phase behavior, and its superior performance over linear PI controllers was demonstrated through simulations. The nonminimum phase behavior in the column occurs due to a competition between a favorable reaction in the column and an unfavorable distillation in the reboiler. This may be a common phenomenon in reactive distillation columns where the desired product is withdrawn at the bottom from the reboiler, and the proposed method in this article provides an approach for addressing the nonlinear control of such columns.

Acknowledgment

Financial support for this work from the National Science Foundation, grant CTS-9320402, is gratefully acknowledged.

Literature Cited

Agreda, V. H., L. R. Partin, and W. H. Heise, "High-Purity Methyl Acetate via Reactive Distillation," *Chem. Eng. Prog.*, **86**, 40 (1990).

Alejski, K., and F. Duprat, "Dynamic Simulation of the Multicomponent Reactive Distillation," *Chem. Eng. Sci.*, **51**, 4237 (1996).

Balasubramhanya, L. S., and F. J. Doyle, III, "Nonlinear Model-Based Control of a Batch Reactive Distillation Column," *Preprints of DYCOPS-5,* Corfu, Greece, p. 123 (1998).
Baldon, J. L., J. J. Strifezza, M. S. Basualdo, and C. A. Ruiz, "Control Policy for the Startup, Semi-Continuous and Continuous Operation of a Reactive Distillation Column," *Preprints of ADCHEM '97,* Banff, Canada, p. 125 (1997).
Barbosa, D., and M. F. Doherty, "Design and Minimum-Reflux Calculations for Double-Feed Multicomponent Reactive Distillation Columns," *Chem. Eng. Sci.*, **43**, 2377 (1988a).
Barbosa, D., and M. F. Doherty, "Design and Minimum-Reflux Calculations for Single-Feed Multicomponent Reactive Distillation Columns," *Chem. Eng. Sci.*, **43**, 1523 (1988b).
Barbosa, D., and M. F. Doherty, "The Influence of Equilibrium Chemical Reactions on Vapor-Liquid Phase Diagrams," *Chem. Eng. Sci.*, **43**, 529 (1988c).
Brenan, K. E., S. L. Campbell, and L. R. Petzold, "Numerical Solution of Initial-Value Problems in Differential-Algebraic Equations," Classics in Applied Mathematics, Society for Industrial and Applied Mathematics, Philadelphia (1996).
Buzad, G., and M. F. Doherty, "Design of Three-Component Kinetically Controlled Reactive Distillation Columns Using Fixed-Point Methods," *Chem. Eng. Sci.*, **49**, 1947 (1994).
Chang, Y. A., and J. D. Seader, "Simulation of Continuous Reactive Distillation by a Homotopy-Continuation Method," *Comput. Chem. Engng.*, **12**, 1243 (1988).
Ciric, A. R., and D. Gu, "Synthesis of Nonequilibrium Reactive Distillation Processes by MINLP Optimization," *AIChE J.*, **40**, 1479 (1994).
Ciric, A. R., and P. Miao, "Steady State Multiplicities in an Ethylene Glycol Reactive Distillation Column," *Ind. Eng. Chem. Res.*, **33**, 2738 (1994).
Corrigan, T. E., and J. H. Miller, "Effect of Distillation on a Chemical Reaction," *Ind. Eng. Chem. Proc. Des. Dev.*, **7**, 383 (1968).
DeGarmo, J. L., V. N. Parulekar, and V. Pinjala, "Consider Reactive Distillation," *Chem. Eng. Prog.*, **88**, 43 (1992).
Doherty, M. F., and G. Buzad, "Reactive Distillation by Design," *Trans. IChemE*, **70**, 448 (1992).
Doyle III, F. J., F. Algöwer, and M. Morari, "A Normal Form Approach to Approximate Input-Output Linearization for Maximum Phase Nonlinear SISO Systems," *IEEE Trans. Automat. Contr.*, **AC-41**, 305 (1996).
Eckert, E., and M. Kubíček, "Modeling of Dynamics for Multiple Liquid-Vapor Equilibrium Stage," *Chem. Eng. Sci.*, **49**, 1783 (1994).
Espinosa, J., E. Martínez, and G. Pérez, "Dynamic Behavior of Reactive Distillation Columns. Equilibrium Systems," *Chem. Eng. Comm.*, **128**, 19 (1994).
Espinosa, J., P. Aguirre, and G. Pérez, "Some Aspects in the Design of Multicomponent Reactive Distillation Columns Including Nonreactive Species," *Chem. Eng. Sci.*, **50**, 469 (1995).
Gehrke, V., and W. Marquardt, "A Singularity Theory Approach to the Study of Reactive Distillation," *Comput. Chem. Engng.*, **21 S**, S1001 (1997).
Grosser, J. H., M. F. Doherty, and M. F. Malone, "Modeling of Reactive Distillation Systems," *Ind. Eng. Chem. Res.*, **26**, 983 (1987).
Güttinger, T. E., and M. Morari, "Predicting Multiple Steady States in Distillation: Singularity Analysis and Reactive Systems," *Comput. Chem. Engng.*, **21 S**, S995 (1997).
Hauan, S., T. Hertzberg, and K. M. Lien, "Why Methyl Tert-Butyl Ether Production by Reactive Distillation May Yield Multiple Solutions," *Ind. Eng. Chem. Res.*, **34**, 987 (1995).
Isidori, A., and C. I. Byrnes, "Output Regulation of Nonlinear Systems," *IEEE Trans. Automat. Contr.*, **AC-35**, 131 (1990).
Jacobs, R., and R. Krishna, "Multiple Solutions in Reactive Distillation for Methyl Tert-Butyl Ether Synthesis," *Ind. Eng. Chem. Res.*, **32**, 1706 (1993).
Jelínek, J., and V. Hlavàček, "Steady State Countercurrent Equilibrium Stage Separation with Chemical Reaction by Relaxation Method," *Chem. Eng. Comm.*, **2**, 79 (1976).
Kravaris, C., and P. Daoutidis, "Nonlinear State Feedback Control of Second-Order Nonminimum-Phase Nonlinear Systems," *Comput. Chem. Engng.*, **14**, 439 (1990).
Kravaris, C., M. Niemiec, R. Berber, and C. B. Brosilow, "Nonlinear Model-Based Control of Non-Minimum Phase Processes," *Preprints of NATO Advanced Study Institute on Nonlinear Model Based Process Control,* Antalya, Turkey, p. 253 (1997).
Kumar, A., and P. Daoutidis, "A DAE Framework for Modeling and Control of Reactive Distillation Columns," *Preprints of 4th IFAC Symp. on Dynamics and Control of Chemical Reactors, Distillation Columns and Batch Processes,* Helsingor, Denmark, p. 99 (1995a).
Kumar, A., and P. Daoutidis, "Dynamic Modeling and Analysis of a Reactive Distillation Column," *Preprints of 1995 AIChE Separation Division's Topical Conference on Recent Developments and Opportunities,* AIChE Meeting, Miami Beach, FL (1995b).
Kumar, A., and P. Daoutidis, "Feedback Control of Nonlinear Differential-Algebraic-Equation Systems," *AIChE J.*, **41**(3), 619 (1995c).
Lichtenstein, H. J., and G. H. Twigg, "The Hydration of Ethylene Oxide," *Trans. Faraday Soc.*, **44**, 905 (1948).
Moe, H. I., S. Hauan, K. M. Lien, and T. Hertzberg, "Dynamic Model of a System with Phase- and Reaction Equilibrium," *Comput. Chem. Engng.*, **19 S**, S513 (1995).
Nijhuis, S. A., F. P. J. M. Kerkhof, and A. N. S. Mak, "Multiple Steady States During Reactive Distillation of Methyl Tert-Butyl Ether," *Ind. Eng. Chem. Res.*, **32**, 2767 (1993).
Pekkanen, M., "A Local Optimization Method for the Design of Reactive Distillation," *Comput. Chem Engng.*, **19 S**, S235 (1995).
Pisarenko, Y. A., O. A. Epifanova, and L. A. Serafimov, "Steady States for a Reaction-Distillation Column with One Product Stream," *Theor. Found. Chem. Eng.*, **21**, 281 (1988).
Rév, E., "Reactive Distillation and Kinetic Azeotropy," *Ind. Eng. Chem. Res.*, **33**, 2174 (1994).
Roat, S. D., J. J. Downs, E. F. Vogel, and J. E. Doss, "The Integration of Rigorous Dynamic Modeling and Control System Synthesis for Distillation Columns: An Industrial Approach," *Chemical Process Control—CPC III,* M. Morari and T. J. McAvoy, eds., Elsevier Science, New York, p. 99 (1986).
Ruiz, C. A., M. S. Basualdo, and N. J. Scenna, "Reactive Distillation Dynamic Simulation," *Trans. IChemE*, **73**, 363 (1995).
Sørensen, E., S. Macchietto, G. Stuart, and S. Skogestad, "Optimal Control and On-Line Operation of Reactive Batch Distillation," *Comput. Chem. Engng.*, **20**, 1491 (1996).
Ung, S., and M. F. Doherty, "Synthesis of Reactive Distillation Systems with Multiple Equilibrium Chemical Reactions," *Ind. Eng. Chem. Res.*, **34**, 2555 (1995a).
Ung, S., and M. F. Doherty, "Vapor-Liquid Phase Equilibrium in Systems with Multiple Chemical Reactions," *Chem. Eng. Sci.*, **50**, 23 (1995b).
Wright, R. A., and C. Kravaris, "Nonminimum-Phase Compensation for Nonlinear Processes," *AIChE J.*, **38**, 26 (1992).

Manuscript received Dec. 23, 1997, and revision received Oct. 21, 1998.